Self-archived version of the article published in Desalination

G. Campisi, A. Cosenza, F. Giacalone, S. Randazzo, A. Tamburini and G. Micale

Desalination of oilfield produced waters via reverse electrodialysis: a techno-economical assessment.

Desalination, Volume 548, 2023, 116289, ISSN 0011-9164,

https://doi.org/10.1016/j.desal.2022.116289

Desalination of oilfield produced waters via reverse electrodialysis: a techno-economical assessment.

Giovanni Campisi[a,b], Alessandro Cosenza[a,b], Francesco Giacalone[a], Serena Randazzo[a,b], Alessandro Tamburini[*a,b] and Giorgio Micale[a,b]

[a]*Dipartimento di ingegneria, Università degli Studi di Palermo (UNIPA), viale delle Scienze Ed.6, 90128 Palermo, Italy*
[b]*Consorzio Interuniversitario Nazionale per la Scienza e Tecnologia dei Materiali (INSTM), via G. Giusti 9, 50121 Firenze, Italy*

** Corresponding Author.*
E-mail address: alessandro.tamburini@unipa.it

Keywords

Produced waters, wastewater, desalination, reverse electrodialysis, assisted reverse electrodialysis, techno-economic analysis

Abstract

Produced waters (PWs) are oilfield waste streams rich in minerals and hydrocarbons whose production rate is largely increased in last decades following the corresponding increase of energy demand. The high salinity level of PWs inhibits the adoption of cheap biological treatments. Also, desalination techniques based on osmotic membranes would require severe pre-treatments. As an alternative, Reverse ElectroDialysis (RED) and Assisted Reverse ElectroDialysis (ARED) are here proposed for the first time to reduce the salinity level of PWs. RED may also guarantee an operation cost reduction thanks to its energy generation. An ad-hoc model for RED and ARED is here developed in order to deal suitably with PWs. This is done by a calibration and validation with

experimental data purposely collected via RED and ARED units fed by real PWs. The model is integrated with economical equations and a techno-economic analysis is carried out in order to identify the best configuration for the desalination purposes. Results suggest that ARED operation mode is the best option guaranteeing a minimum in the controlled dilution cost corresponding to a 1.32 € per m^3 of PWs treated, thus leaving room for an affordable future implementation of more sophisticated treatment chains based on bioremediation.

1 Introduction and literature review

Crude oil and natural gas drilling are the principle sources of energy and profit for many countries and their products are the basis for the major chemical industrial processes. Although scientists are looking for renewable alternatives to oil and natural gas exploitation, the latter is expected to remain highly profitable in the near future. Given also the continuous and increasing demand of crude oil, it is mandatory to find a way to treat the large volume of wastes generated during its extraction, whose liquid fraction is up to 80% of the total wastes. These wastewaters are known as Produced Waters (PWs) and represents a crucial issue for extraction companies, because of their high salinity and the presence of organic pollutants.

In order to reduce tackle this issue, the three-tiered pollution prevention hierarchy approach has been proposed [1]:

1- Employing technologies to minimize produced water extraction;

2- Reuse and recycle of produced water;

3- If neither of the previous strategies are practical, the disposal of the produced water is the final option.

Technologies avoiding PWs production include the use of polymer gel or downhole water separators, but their adoption is not always possible [2]. In offshore platforms, PWs are conventionally treated in oil-water separators and then discharged into the sea. Conversely, in onshore applications, a reuse attempt of this waste includes the reinjection of the water into its well or other wells to enhance the

oil extraction [3]. This strategy is actually the most widely used in industrial practice, however, the reinjection requires soft treatment for reducing fouling and bacteria growth, and the handling of huge volumes of water. Moreover, for very long storing periods, the stored PW may pollute the underground water [2], [4]. Stringent regulatory standards for the PWs discharge are adopted in each country. EU Water Framework Directive approved in 2000 (2000/60/EC) is committed to a "zero discharge" strategy against the aquatic pollution and most oil and gas companies in the world are moving towards that direction [3], [5]. For each barrel of crude oil extracted, 3 barrels of produced water come up on average, and this value is going to increase with the plant age [1]. Given the huge volumes of PWs extracted during the oil well life, the handling and disposal of this waste stream has a significant additional cost in the managing of the well. The disposal cost varies between the 5% and 19% of the total capital cost, and its management from 7 to 52% of the lease operating expenditures, depending on the well location [6]. As alternatives to PWs reinjection, an option can be the reuse in the oil and gas operation (for example for drilling), or after suitable treatments the use in irrigation, animal breeding and as drinking water [7]. Clearly, each option of reuse requires specific and regulated characteristics of the water, thus a suitable treatment strategy is compulsory. These treatment chains are typically devoted to the removal of dispersed oil, grease and solids, dissolved gases, naturally occurred radioactive materials sometimes [8], to the disinfection, to the desalination and to the softening of PWs [9]. Membrane filtration has proven to be a technology particularly suitable in the PW treatment [10]. Microfiltration (MF) and Ultrafiltration (UF) modules exhibit pores size in the range of 0.1 – 3 μm and 0.01 – 0.1 μm respectively. They are typically used for the solids removal and turbidity reduction, up to the separation of oil, bacteria, viruses, heavy hydrocarbons, colloids and organic molecules for the case of fine UF. Polymeric and ceramic modules are used, in both cross-flow and dead-end filtration modes [11]–[13].

In all the possible treatment processes, typical or innovative, the high salinity of these kind of stream represents a crucial issue. Biological treatment is one of the cheapest and most efficient technology to treat organically polluted wastewaters. Traditionally used for urban wastewaters, biological

treatments cannot be applied when wastes exhibited a high salinity [14]. In addition to that, high salinity streams are corrosive and requires the use of special materials thus increasing the construction costs. Moreover, most of the proposed reuses of the PWs, such as irrigation-water or process-water, requires a low salt content [3].

Several methods have been applied to reduce the salinity of the PWs so far. Among them, thermal technologies are the mostly adopted. Multistage flash (MSF) distillation is typically used for seawater desalination but it has been proposed also to deal with PWs [15]. MSF represents a robust technology, but requires a rigorous pre-filtration and a pre-treatment to prevent scaling phenomena that increase the operative costs [15], growing the total costs per unit up to 1.17 €·m^{-3} [2]. Multi-effect distillation (MED) is considered a suitable process for PW treatment, with a capital cost of about 1,530-2,020 €·m^{-3}·day [2]. However, it requires several pre-treatments, inhibitors and acid dosing in order to avoid scaling [3]. In vapour compression distillation (VCD) the vapour generated is mechanically or thermally compressed and the heat of condensation is exploited as heat source [15]. The typical costs of this technology amount to 0.65 € m^{-3} for seawater [2], but this cost is expected to increase due to the higher salinity of PWs. Hybrid MED-VCD is a recent process suitable for PW desalination, used to increase the energy efficiency and the water recovery [3]. Here, the capital cost is almost 1,531 €·m^{-3}·day and the operating costs are variable and affected by the energy consumption of the unit [2]. However, thermal evaporation technologies are the most expensive [15], [16], (even, prohibitively expensive for small scale plants) and this is why other processes, as the membrane-based ones, have been taken into account recently. As a matter of fact, membrane processes are generally cheaper and less energy-intensive, and for this reason have been the mostly used in recent years [15], [17].

Reverse osmosis (RO) is the mostly adopted pressure driven membrane process to desalinate a stream with a capital cost between 776 and 1,812 € m^{-3}day [15] with variable operative costs, strongly dependent on PW salinity, utilities costs and on the pre/post-treatment steps needed. Several studies have demonstrated as RO processes are the most efficient for ions removal from salty streams [18], [19]. However, the RO membranes presents a strong sensitivity to fouling, which causes multiple

adverse effects on the systems performances [21]. In particular, biofouling is considered the most challenging issue to tackle, as during operation microorganism can quickly colonize the membrane surface. Membrane distillation (MD) is a thermally driven membrane process that utilizes low-grade heat to drive the separation between solvent and solutes and has been already proposed for the PW desalination [22]. MD may easily deal with very high salinity streams but pre-treatments are required, especially in order to completely remove suspended solids and surfactants present in the PW feed [15]. On the other hand, residual organic compounds and dissolved gases are transported through the membrane and could contaminate the distillate solution [15], [22], [23].

It is worth noting that the cost for desalinating PWs might be very different, depending on PWs features (e.g. salinity level, kind of pollutants), geographical position of the extraction situ (e.g. onshore, near the sea, etc), legislative constraints (e.g. constraints on cut-off values for disposal), the treatment chain adopted (whose which, desalination represents one step), etc.

Electro-membrane processes have an important role in low-salinity desalination applications. The majority of industrial plant of electrodialysis (ED), electrodialysis reversal (EDR) and electro-deionization (EDI) deals with brackish water, with a capacity ranging between few tens of m^3 day^{-1}, to 10,000 m^3 day^{-1} [24]. ED is a well-known technology applied in various industrial fields such as in the food sector [25], ultrapure water production [26], heavy metals removal [27] and studied in several innovative application, such as the tertiary treatment of municipal wastewaters [28] and as a pre-treatment step for the RO seawater desalination [29].

Among emerging technologies, Reverse ElectroDialysis (RED) can take advantage of this high salinity in order to valorise PWs by producing electric energy as already demonstrated by Cosenza et al. [30]. Interestingly, while RED is producing energy, it intrinsically performs a controlled dilution of the PWs and could be adopted as a pre-treatment for downstream treatment steps based on bioremediation.

In this context of controlled dilution of salty streams, Assisted Reverse Electrodialysis (ARED) is a novel technique which is attracting a growing interest in the desalination community. As a difference

from standard RED, in ARED the spontaneous ion passage from the concentrate stream to the dilute stream is “assisted” (i.e. enhanced) by applying an external voltage. As a consequence, in ARED no energy is generated, rather, it is consumed to assist the controlled dilution [31], [32]. On the other hand, a lower membrane area is required for the desalination, thus resulting into lower capital costs [32].

RED and ARED have been proposed in different schemes to pre-desalinate streams before a further treatment [29], [33]–[35]. Gurreri et al. [29] tested ED-ED-RO, ED-RO and RED (in short circuit conditions)-ARED-RO configurations finding that the energy consumption was about 5.6-8.4 kWh m^{-3} in the firstly mentioned configuration, while it reduced to about 4.1 kWh m^{-3} with the simpler ED-RO system. The lowest energy consumption (about 3.5 kWh m^{-3}) was found for the case of ARED, demonstrating that this process represents an interesting alternative in the fields of desalination and wastewater treatment. La Cerva et al. [33] used a model to evaluate the performances and costs of ARED-RO and ED-RO and compare them with a stand-alone RO system. ARED-RO was found to require a lower energy consumption for a wide range of applied external voltage, with a maximum cost saving of about 7.5%. Conversely, in the ED-RO system the energy consumption in the ED pre-treatment exceeded the energy saving of the following RO step.

Since its proposal by Pattle [36], a number of research efforts have been devoted to the study of the RED process and to the modelling of its fundamentals. The work by Veerman et al. [37] reported certainly the most famous RED mathematical model in the literature for river water-seawater. The model was simple yet sufficiently reliable and based on thermodynamics equations for the cell pair voltage, electric and transport equations, all coupled with mass balances. Some years later, Tedesco et al. [38] proposed a more sophisticated multi-scale approach extending the Veerman et al. model [37] to the case of more concentrated solutions such as brines and bitterns. This model was then further developed thanks to the coupling with suitable correlations deriving from CFD simulations in order to predict the concentration polarization phenomena at the channel scale [39], [40].

More recent and sophisticated models (multi-ionic models included) have been proposed to address the impact of parasitic currents [41] and of ions different than the most abundant Na^+ and Cl^- [42], [43] on the unit performance. A recent comparison of all models focused on RED is proposed by Tristàn et al. [44]. An analysis of RED performance scenarios (obtained by varying properties of solutions and geometric stack details) is presented by Ortiz-Martinez et al. [45]. Ortiz-Imedio et al. [46] studied the behaviour of a RED stack unit, with different feed solutions, as seawater-wastewater treatment plant effluent and brines-brackish water and obtained a power of 0.66 and 1.6 W respectively.

Surprisingly, although several experimental works have been devoted to studying RED with solutions different than the traditional seawater-river water, there are practically no modelling works dealing with PWs. To the authors' knowledge, RED is proposed here for the first time as a controlled dilution method for reducing the salinity of PWs. Ad-hoc models are essential to properly assess the technical and economic feasibility of a given technology especially when alternative scenarios are investigated. With this respect, the present work is aimed at filling this gap for the case of PWs. An ad hoc model was developed to predict the performance of RED and ARED units fed by PWs. Once the model has been validated with purposely collected experimental data, it was used to perform a techno-economic analysis of the process to assess its feasibility. The idea is that of adopting RED/ARED as a controlled dilution step for the PWs in order to make them compliant with downstream bioremediation approaches devoted to the organic matter removal. To this purpose, considering that biological reactors requires low salinities for the bacteria growth [14], a target concentration of 20 g L^{-1} has been identified as the maximum value at which the removal of the organic pollutants with biological treatments is still feasible [47], [48].

2 RED/ARED Model

In RED and ARED, the mixing of two saline solutions at different concentrations occurs according to the spontaneous direction, i.e., the ions move from the concentrated solution compartment (high

concentration solution, HC), to the diluted one (low concentration solution, LC) through Ionic Exchange Membranes (IEMs). Cationic and Anionic Exchange Membranes (CEMs and AEMs) allow the passage of only positive and negative ions respectively. CEMs and AEMs are piled in an alternate way and separate by net spacers which give dimensional stability to the channels hosting the solutions. The combination of one AEM, one CEM and two spacer-filled channels (where the concentrate and the dilute streams are forced to flow) represents the repetitive unit of the RED/ARED stack and is named cell-pair (Fig. 1).

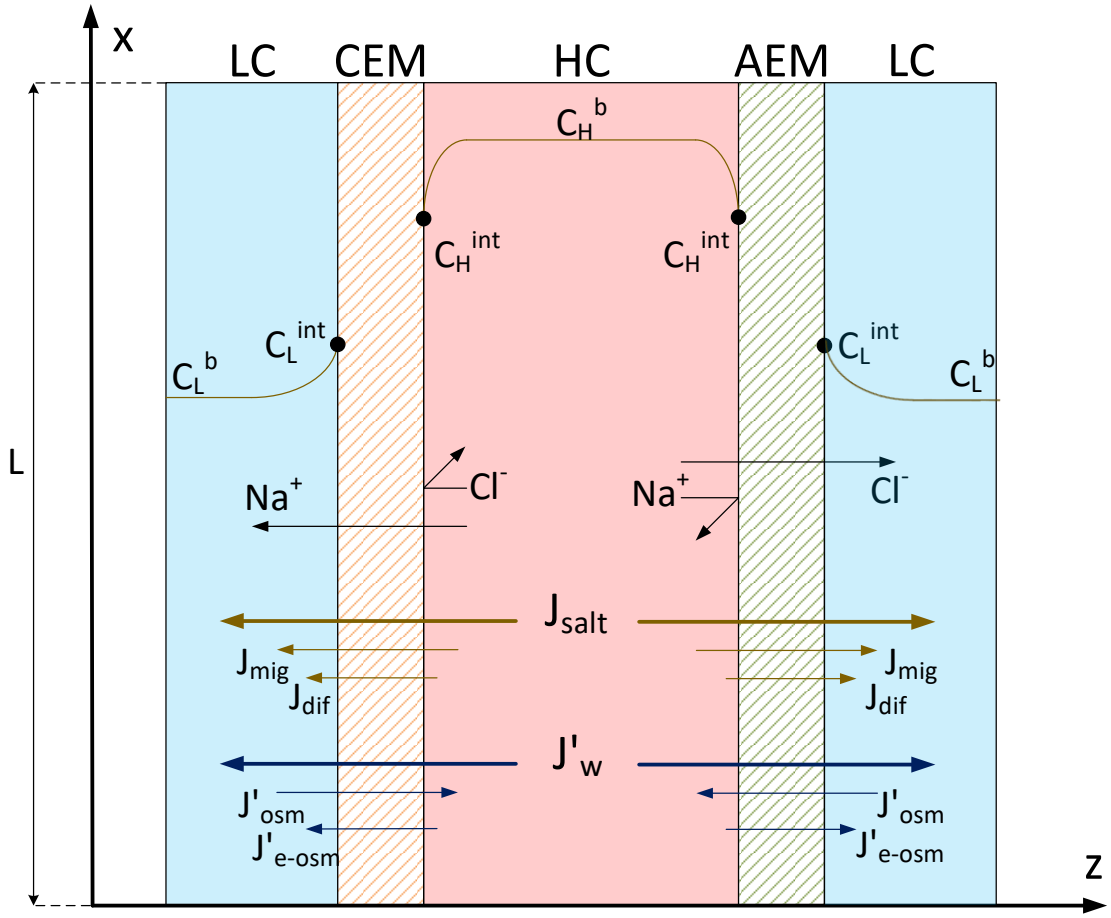

Fig. 1 Schematic representation of a cell pair of a RED/ARED stack. The concentration profiles of salt, the ions direction across the membranes and the direction of the salt and water fluxes in the Low and High concentration compartments (respectively LC and HC) are reported. Look at Appendix I for the equations of fluxes and at section 2.2.

The operation of the system in RED or ARED condition is represented in Fig. 2. When the system is fed by the solutions and the external circuit is open, the open circuit voltage (E_{OCV}) is measured between the electrodes, and no current circulates in the system. By closing the electric circuit, i.e. by

connecting the electrodes to an external load, and progressively reducing the external load value, the voltage is progressively reduced, and a progressively higher ionic current spontaneously occurs in the system. The unit is working in RED condition with the ions transferred from the high solution to the low solution. At the electrodes, the ionic current is converted into an electric current circulating in the external circuit. The product of the electric current and the stack voltage is the power generated by the unit. The maximum current spontaneously produced by the system is the short circuit current (I_{SC}), corresponding to an electric voltage and a power generated equal to 0. A higher ionic current can be induced in the system by applying an external electric field in the same direction as the natural flux of ions. In this condition, the system operates in ARED mode with a certain consumption of electric power given by the product of the applied voltage and the electric current.

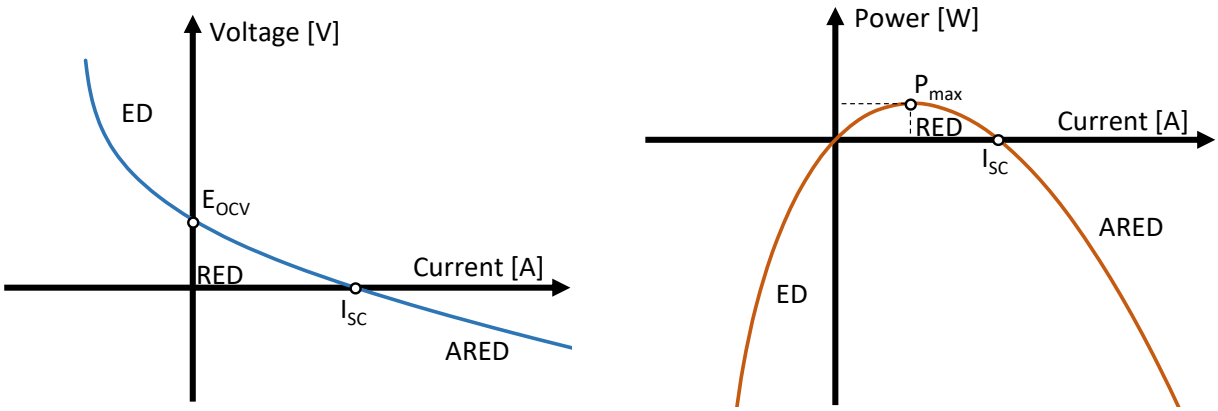

Fig. 2 Schematic representation of Voltage (on the left) and Power (on the right) trends vs. the current.

2.1 Simplified assumptions

The proposed multiscale model for RED/ARED is based on the following simplifying assumptions:

1 The model equations are discretized along the main flow direction only (see x-axis in Fig. 1), while polarization factors are adopted to account for concentration variation along the cross-stream direction (z-axis in Fig. 1);

2 The flow field is assumed identical in each compartment. In other words, flow rate in each channel is identical, independently of the cell pair position;

3 The short-cut currents through the manifolds of the stack are not taken into account. Parasitic currents are known to play a crucial role when a high number of cell pairs is adopted and when feed solutions are very conductive (e.g. brines) because low resistance pathways are preferred compared to the desired current direction [41]. Their impact can be significantly reduced by suitably choosing the channels and manifolds design features.

4 The feed solutions are modelled as streams composed of sodium chloride only (see Appendix II for solution properties and correlations). However, the main membrane properties (e.g. permselectivity and electrical resistance) adopted in the model have been experimentally obtained (see section 3.2) with real PWs.

2.2 Model main equations

For the sake of brevity, only the main equations adopted in the model and related to the case of RED technology are reported in this section. All the other equations are reported in Appendix I. Full details of the model can be found in [37], [38], [40], [49].

The salinity gradient over the IEMs of the whole stack generates an electric voltage defined by the Nerst equation (Eq. 1).

$$E_{OCV} = 2\ \mathrm{PS}_{av}\ N_{cp}\ \frac{R_g T}{zF}\ \ln\frac{\gamma_H\ c_H^b}{\gamma_L\ c_L^b} \quad \textbf{(1)}$$

where N_{cp} is the number of cell pairs, PS_{av} is the average permselectivity of the membranes (i.e. the arithmetic mean between *CEM* and *AEM*), R_g is the gas constant, *T* the absolute temperature of the process, *F* is the Faraday constant, *z* is the ion charge of the salt (for NaCl is equal to 1), *c* and γ are the bulk molar concentrations and the activity coefficients of the solution. The subscripts *H* and *L* refer to the High salinity solution and the Low salinity solution.

When the external circuit is closed and a current density *i* is circulating into the system, a salt flux occurs. With reference to a differential control volume along the x-axis, the following differential mass balances are solved:

$$\frac{dQ_L c_L}{b\ dx} = J_{salt}(x) - \ c_L(x)\ J'_w(x) \quad \textbf{(2)}$$

$$\frac{dQ_H c_H}{b\,dx} = -J_{salt}(x) + c_H(x)\,J'_w(x) \quad \textbf{(3)}$$

where Q and c are the volumetric flow rate and the concentration of the 2 solutions, respectively, b is the width of the stack (the length along the y-axis) and J_{salt} and J'_w are the total molar flux of salt and volumetric flux of water, respectively. As shown in Fig. 1, the total salt flux J_{salt} is composed of the sum of two terms, the migrative flux and the diffusive one (see Appendix I). The migrative flux of ions is directed according to the current of the stack and can be described by Faraday's law, conversely, the diffusive flux is defined by Fick's law. The second addendum on the right hand side of Eqs. (2) and (3) is related to the water fluxes (i.e. osmotic and electro-osmotic fluxes) whose mathematical expressions are detailed in [37].

The current circulating in the system generates a concentration variation both along the streamwise (i.e. along the x-axis) and the cross-stream (i.e. along the z-axis) direction. These concentration variations correspond to a salinity gradient reduction and are typically regarded as non-ohmic resistances [40], [49]. The former is larger, the higher the residence time of the solution within the stack. It is intrinsically taken into account by the present model which is discretized along the x-axis direction in N_k elements. The latter is the outcome of concentration polarization phenomena and is accounted for by the correction factor θ_{sol} (one per each stream), known as polarization coefficient whose value ranges between 0 and 1. These two non-ohmic resistances are taken into account in Eq. (4) where the electric potential over a cell-pair is reported for a generic k-th element:

$$E_{cell}(k) = 2\,PS_{av}(k)\,\frac{R_g T}{F}\,ln\left(\theta_H(k)\theta_L(k)\,\frac{c_H^b(k)\,\gamma_H(k)}{c_L^b(k)\,\gamma_L(k)}\right) \quad \textbf{(4)}$$

The current density i is calculated as follows (Eq. 5):

$$i(k) = \frac{E_{cell}(k) - {E_{stack}}/{N_{cp}}}{R_{cell}(k) + R_{blank}} \quad \textbf{(5)}$$

where $R_{cell}(k)$ is the sum of the ohmic resistances within a cell pair (comprehensive of solution compartments and membrane resistances), R_{blank} is the electrical resistance due to the electrode compartments and to the end membrane, E_{stack} is the fixed electric potential difference at the

electrodes. The current is expressed as a function of E_{stack} in order to easily describe both RED and ARED operation modes.

By solving the model equations at each *k-th*, the gross power produced/consumed by the stack can be calculated via equation (Eq. 6):

$$P_{gross} = E_{stack} \sum_{1}^{N_k} b\Delta x \cdot i(k) = E_{stack} \; I_{stack} \quad \textbf{(6)}$$

where I_{stack} is the current transiting in the external circuit. Notably, P_{gross} is positive when energy is produced by the system (RED operation mode), conversely, it is negative when energy is consumed (ARED operation mode).

Adopting a multi-scale model is a good approach to deal with processes where different important phenomena occur at the same time but at a different scale. The model here adopted is also able to provide local and overall information with minimum time and computational requirements. The model is based on a semi-empirical approach as it requires experimental information on membrane perm-selectivity and electrical resistance. On the one hand, this allows the model to be well calibrated with experiments, thus leading to robust and reliable results. On the other hand, when different membranes and feed-solutions are to be employed (as it occurs in the present work dealing with PWs), a new calibration or new experimental-based correlations are needed.

2.3 Economic Model

In order to assess the costs of applying RED as a controlled dilution step for PWs, an economic model is implemented. Both capital and operating costs are estimated. To this aim, for given operating conditions and plant size, the main outputs of the mathematical model, in terms of gross power required or produced by the RED/ARED unit and pumping power, are used to evaluate the cost required per each cubic meter of PW.

Main economic parameters adopted as inputs for the engineering economic analysis are reported in Tab. 1.

Tab. 1 Economic parameters.

Plant lifetime $\boldsymbol{t}$	20	year
Discount rate $\boldsymbol{r}$	3	%
Working hour	8000	h $\cdot year^{-1}$
RED membrane lifetime $\boldsymbol{t_m}$	4	year
Electricity cost $\boldsymbol{C_{electricity}}$	0.12	€ $\cdot kWh^{-1}$
Water cost $\boldsymbol{C_{water}}$	0.0 - 0.3	€ $\cdot m_W^{-3}$

The Fixed Capital Investment (FCI) is calculated as the sum of direct and indirect costs as follows:

$$FCI = C_m + C_{electrode} + C_{casing} + C_{spacer} + C_{pump} + C_{piping} + C_{labour} \quad \textbf{(7)}$$

The value of each addendum is declared in Tab. 2. As it can be seen there, some of these values are referred to a geometrical feature of the stack: for instance the total active membrane area ($m^2_{IEMs} = 2\ N_{cp} \cdot A_m$ where A_m is the area of a single membrane) or the active area of the electrode ($m^2_{electrode}$ is the active area of each electrode assumed equal to A_m).

As far as the costs of the membranes (C_m) is concerned, different values has been proposed so far. A cost of 15 € $\cdot m^{-2}_{IEMs}$ is generally considered a more than reasonable value, while a value of 4 € $\cdot m^{-2}_{IEMs}$ is often adopted as a future cost [50], [51] which is expected to benefit from both technological developments and the spreading of RED and ED technologies at world level. For the sake of the present work, an intermediate value of 10 € $\cdot m^{-2}_{IEMs}$ is considered. Note that in other works FCI is called CAPital EXpenditures (Capex).

Tab. 2 Main cost items for the economic analysis.

Membranes cost $\boldsymbol{C_m}$	10	€ $\cdot m^{-2}_{IEMs}$	[50], [51]
Electrode cost $\boldsymbol{C_{electrode}}$	500	€ $\cdot m^{-2}_{electrodes}$	[51]
Casing cost $\boldsymbol{C_{casing}}$	2	€ $\cdot m^{-2}_{IEMs}$	[51]

Spacers cost $\boldsymbol{C_{spacer}}$	5	$€ \cdot m_{IEMs}^{-2}$	[51]
Pump cost $\boldsymbol{C_{pump}}$	$900\left({\mathrm{P_{pump}[W]}}/{300}\right)^{0.25}$	€	[52]
Piping cost $\boldsymbol{C_{piping}}$	$(0.087 + 0.21\mathrm{D_{pipe}[mm]})\mathrm{L_{pipe}[m]}$	€	[52]
Labour cost $\boldsymbol{C_{labour}}$	20% of $equipment\ cost^{(*)}$	€	[50], [53]
Other costs $\boldsymbol{C_{other}}$	4% of FCI	$€ \cdot year^{-1}$	[51]

$^{(*)}\ equipment\ cost = C_m + C_{electrode} + C_{casing} + C_{spacer} + C_{pump} + C_{piping}$

Operating costs (OPerative EXpenditures, Opex) are the sum of maintenance cost and day-to-day operation costs and can be calculated according to Eq. (8).

$$Opex = C_{dil} + C_{pumping} + C_{power} + C_{other} \quad \textbf{(8)}$$

where C_{dil} is the cost related to the fresh water used as diluted solution in the RED/ARED unit, given by the product of the annual flow rate of the fresh water consumed and its specific cost (C_{water}); C_{pump} is the electricity costs needed to pump the solution into the stacks; C_{power} is the electricity costs required to operate the stack in ARED working mode, (of course, when the stack is operated in RED mode, this value is not considered as an Opex but as a revenue). C_{other} includes all the other manufacturing expenditures such as labour, maintenance, etc.

In order to compare directly capital and operating costs (as €·year^{-1}), FCI is annualized and reported as Annualized CAPital EXpenditure (Acapex), elsewhere named Annual Capital Charge (ACC) [54].

$$Acapex = ACC = \frac{r(1+r)^t}{(1+r)^t - 1}\ FCI \quad \textbf{(9)}$$

For easy comparison purposes, both Acapex and Opex are referred to the plant capacity, i.e. are reported as specific cost calculated per cubic meter of PW treated. The total specific cost for the controlled dilution of a cubic metre of PW (m^3_{PW}) is equal to:

$$C_{tot} = \frac{Acapex + Opex}{Q_H\ [m^3 \cdot year^{-1}]} \quad \textbf{(10)}$$

3 Model validation

3.1 Experimental Apparatus and Procedure

In order to make the model capable of suitably predicting the behaviour of a RED/ARED unit fed by real PWs, ad-hoc experiments were performed with a laboratory scale test rig. The aim was that of calibrating the model in terms of membrane resistance ($R_{m,av}$) and permselectivity (PS_{av}).

A lab-scale unit with an active area of 0.1x0.1 m^2 and equipped with 20 cell pairs provided with woven spacers 300 μm thick (Redstack, Sneek, The Netherlands), Fujifilm Type 10 AEM and CEM (Tilburg, The Netherlands), and Fumasep FKS-50 CEM as end-membranes (Fumatech, Bietigheim-Bissingen, Germany) was used. A real PW (coming from European wells) was employed as concentrated stream after a preliminary filtration in a 1 μm cartridge filter. A synthetic aqueous solution composed of NaCl only (0.73 $g \cdot L^{-1}$) was adopted as low concentrated solution. The electrodic rinse solution (ERS) was prepared dissolving in deionized water: (i) 32.9 $g \cdot L^{-1}$ of $K_3[Fe(CN)_6]$ (>99%), (ii) 42.2 $g \cdot L^{-1}$ of $K_4[Fe(CN)_6]$ (>99%) and (iii) 34 $g \cdot L^{-1}$ of NaCl (99.8%) (all chemicals provided by Sigma Aldrich, St. Louis, MO, USA). The overall ohmic resistance of the electrodic compartments along with one end-membrane (i.e. blank resistance) was found equal to 0.0027 $\Omega \cdot m^2$.

Two peristaltic pumps (Leadfluid WT/600/S, He Bei Sheng, China) were used to feed the solutions into the stack with a co-current arrangement. Another peristaltic pump (Seko Kronos 50, Rieti, Italy) was used to recirculate the ERS. The two solutions were fed to the stack with a flow rate of about 180 $mL \cdot min^{-1}$ corresponding to an inlet velocity of about 0.6 $cm \cdot s^{-1}$ within the channels. A sketch of the experimental set-up is shown in Fig. 3.

In order to reproduce the real operation of the system, the stack was operated in ARED mode at a current being 1.6 times larger than the one relevant to short-circuit conditions (I_{SC}). The PW was continuously recirculated in the concentrated channels of the stack while the low channels were continuously fed with a fresh low solution with a concentration of 0.73 $g \cdot L^{-1}$. The stack was operated up to the concentrated solution (30 L) reaches the target value of 20 $g \cdot L^{-1}$.

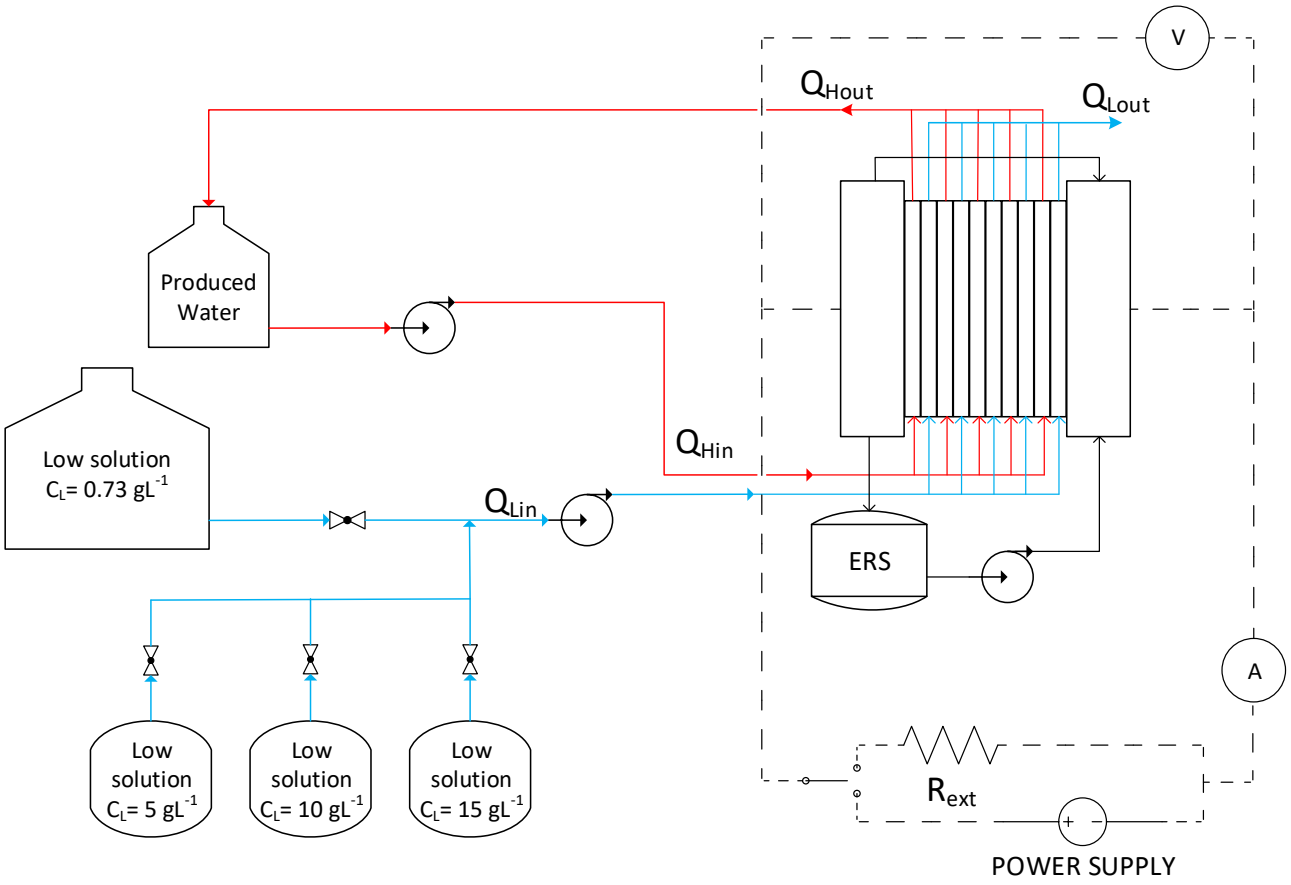

Fig. 3 Sketch of the experimental test-rig adopted in this work.

Periodically, at certain values of PW concentration, the system was switched to RED mode, in order to evaluate the average IEMs resistance and permselectivity at given values of solutions concentration. Thus, the power supply (BK1902B, B&K Precision, B&K Precision, Yorba Linda, California, United States) was disconnected and replaced with an external load (BK,8540, B&K Precision). After membrane conditioning time, RED operability was varied from OCV to SC by step-wise varying the external load connected to the system and measuring the corresponding electric voltage and current. As result post-processing, the OCV measurement was used to determine the average IEMs permselectivity while the slope of the voltage/current curve was used to determine the average stack resistance (R_{stack}).

By assuming $R_{CEM} = R_{AEM}$ and by referring to Eqs. 17-19 of Appendix 1, the average membrane resistance of $R_{m,av}$ can be assessed as follows:

$$R_{m,av} = \frac{1}{2}\left[\frac{A_m}{N_{cp}}\, R_{stack} - R_H - R_L - R_{blank}\right] \quad \textbf{(11)}$$

where R_H e R_L are the electrical resistances of the high and low compartments, respectively. The average Permselectivity (PS) is calculated as the ratio between the E_{OCV} measured and the theoretical one.

For each value of PW concentration, these measurements were repeated for different values of low concentration of 0.73, 5, 10 and 15 g·L^{-1}, in order to obtain a trend of $R_{m,av}$ and PS_{av} as a function of both c_H and c_L.

3.2 Model Calibration and Validation

The calculated values of PS_{av} and $R_{m,av}$ were fitted as a function of c_H and c_L on Matlab® by using polynomial correlations. The experimental correlations for evaluating the average IEM permselectivity and resistance are reported in Eqs. 12 and 13, respectively.

$$PS_{av} = 1.046 - 0.487\, c_H + 0.5318\, c_L + 0.2291\, c_H^2 - 0.3501\, c_H \cdot c_L \quad \textbf{(12)}$$

$$R_{m,av} = 0.001878 - 0.001945\, c_H - 0.00212\, c_L + 0.0007079\, c_H^2 + 0.002566\, c_H \cdot c_L \quad \textbf{(13)}$$

Both correlations present R-square higher than 0.95.

A comparison between experimental and calculated values of PS_{av} and $R_{m,av}$ are reported respectively in Fig. 4 and Fig. 5. In particular, Fig. 4a shows the correlation 3D trend of PS_{av} as a function of c_H and c_L, while Fig. 4b shows the corresponding parity plot. The same information is reported in Fig. 5 for the case of $R_{m,av}$. Moreover, in order to compare the performance of the IEMs evaluated with real PW with the ones when operating in artificial solutions, Fig. 4a and Fig. 5a report also the corresponding values of PS_{av} and $R_{m,av}$ evaluated by experimental correlations reported by Giacalone et al. [51] for the same IEMs operating with solutions composed of water and NaCl only. As expected, when natural PWs are used, PS_{av} values are much lower than in the case of artificial concentrated solutions, especially at high c_H values (see Fig. 4a). Interestingly, the correlation proposed is able to follow the experimental data with a very good agreement with a maximum discrepancy lower than 2.6% (Fig. 4b).

As far as $R_{m,av}$ is concerned, the trend of $R_{m,av}$ as a function c_H and c_L reported in Fig. 5a is quite complex, especially when compared with the trend of IEMs operating with artificial solutions. This is allegedly due to the fact that the proposed correlation here is based on experimental values measured with real PWs containing a plethora of different ions (multivalent ions included), which are known to significantly affect IEM electrical resistance [55]. The parity plot of Fig. 5b shows that the $R_{m,av}$ correlation is quite effective with an error being always below 19%.

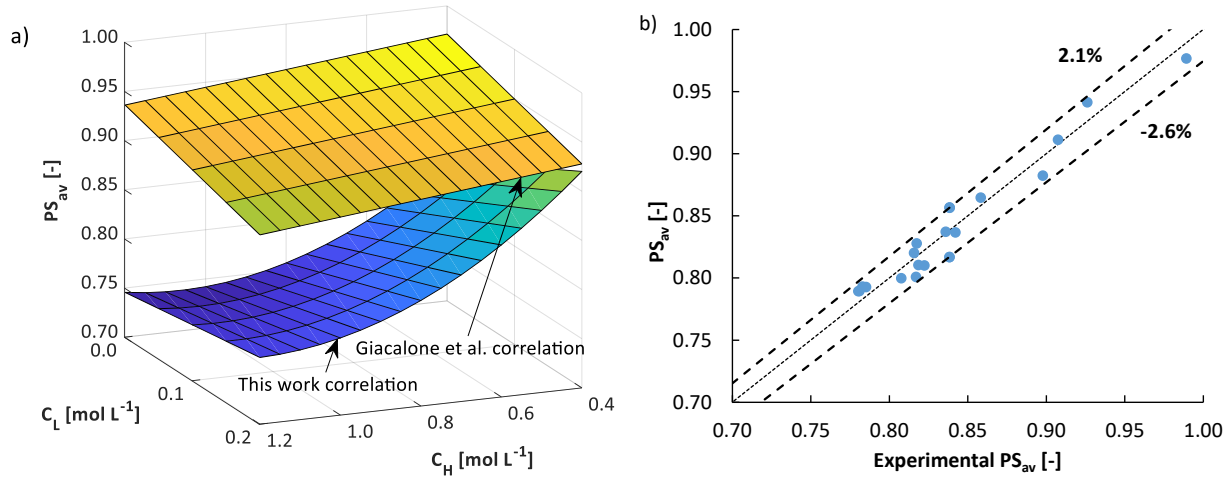

Fig. 4 Comparison between correlations adopted in this work and those in Giacalone et al. [51] for the permselectivity as function of c_H and c_L (a) and the parity plot of this work correlation (b).

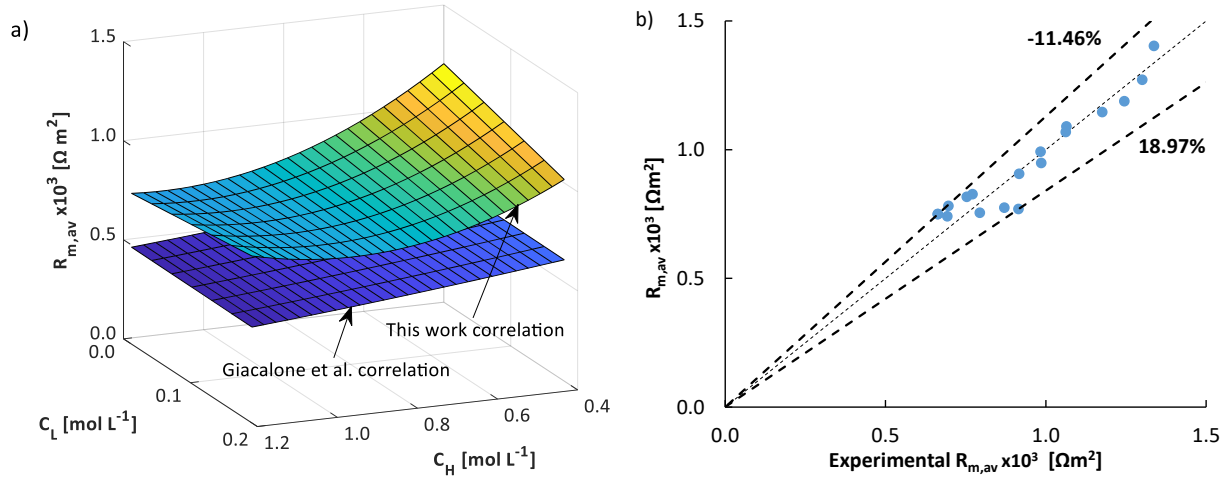

Fig. 5 Comparison between correlations adopted in this work and those in Giacalone et al. [51] for the membrane resistance as function of c_H and c_L (a) and the parity plot of this work correlation (b).

Once obtained, the proposed correlations were implemented in the semi-empirical model briefly described in section 2. Then, for validation purposes, the model predictions were compared with the

corresponding experimental data collected with the set-up reported in section 3.1. In particular, Fig. 6 shows the comparison between experimental results and model predictions for the case of voltage versus current density and power density per cell pairs versus current density trends. Predictions obtained with the model by Giacalone et al. [51] are shown as well for the sake of comparison. As reported in Fig. 6, independently of the concentration of the feed solutions, when PS_{av} and $R_{m,av}$ are not calibrated with PWs, a large discrepancy between model predictions and experimental results can be found, while a very good agreement is obtained when the proposed correlations are implemented. More important, the use of real PWs results in a significant loss of performance of the RED unit with respect to the case of artificial solutions.

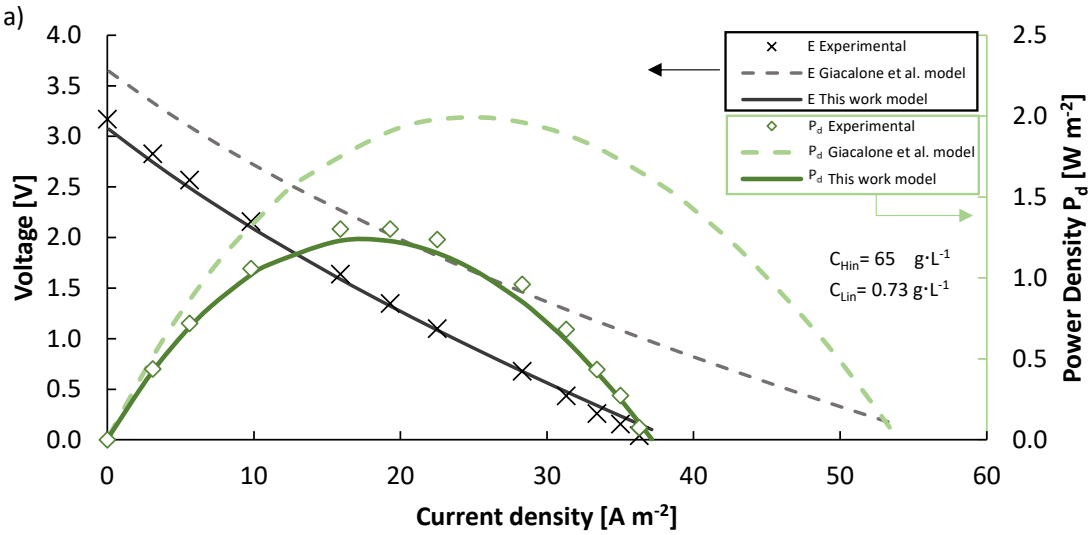

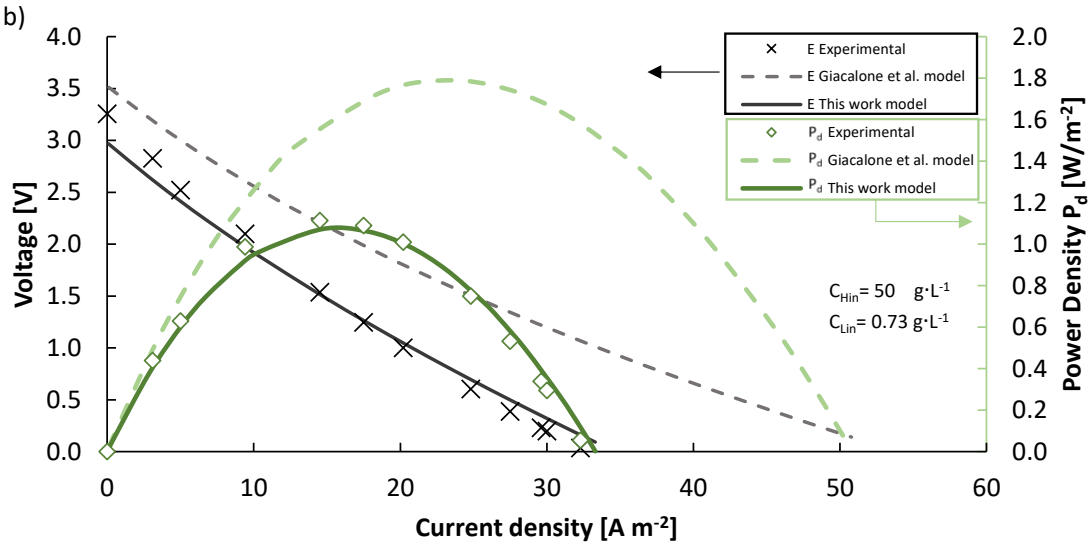

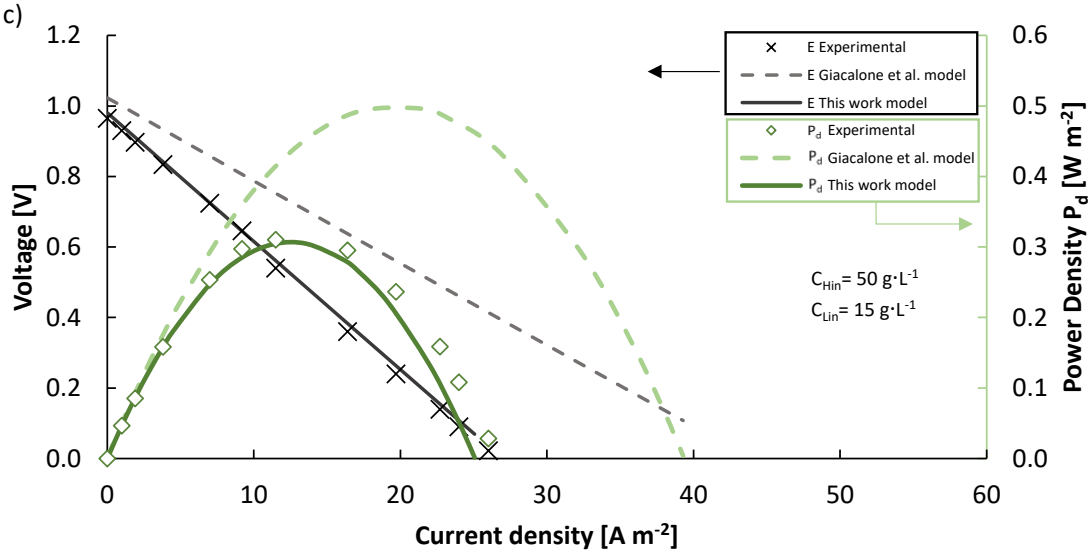

Fig. 6 Voltage vs Current density and Power density per cell pairs vs Current density trends: comparison between experimental data and model predictions. The stack is 0.1x0.1m length with 20 cell pairs and spacers 300µm thick. $v_H = v_L$ =0.6 cm·s^{-1}. a) c_{Hin}=65 g·L^{-1} and c_{Lin}=0.73 g·L^{-1}, b) c_{Hin}=50 g L^{-1} and c_{Lin}=0.73 g·L^{-1} c) c_{Hin}=50 g·L^{-1} and c_{Lin}=15 g·L^{-1}.

4 Results and discussions

A simulation campaign was carried out in order to evaluate the performance and the cost required for diluting PWs down to a target concentration of 20 g·L^{-1} through an industrial-scale RED/ARED unit. Different scenarios were investigated according to the parameters reported in Tab. 3.

Tab. 3 Scenarios configuration for simulative model campaign

Variable	***Scenario 1***	***Scenario 2***	***Scenario 3***	***Scenario 4***	***[-]***
v_{Hin}	0.40	0.60	0.80	1.00	cm·s^{-1}
Q_H	1782	2673	3564	4455	L·h^{-1}
v_{Lin}	0.78	1.17	1.56	1.95	cm·s^{-1}
Q_L	5791.5	8687.3	11583.0	14478.75	L·h^{-1}

In particular, in all the investigated scenarios the stack used is constituted by 500 cell pairs, each one 1 m wide (b), while the stack length (L) is varied for each scenario from 0.5 m up to 4 m. The inlet

concentration of the two solutions were fixed at c_{Hin}=70 g·L^{-1} and c_{Lin}=1 g·L^{-1}. The velocity of the concentrate solution v_{Hin} is increased from scenario 1 to scenario 4 from 0.4 cm·s^{-1} up to 1 cm·s^{-1} (as often suggested in literature [38], [56], [57]), while v_{Lin} is chosen in order to guarantee that, within the investigated range of operating conditions, the concentration of PW exiting the stack complies with the dilution target (i.e. c_{Lout} lower than 30 g·L^{-1}, that corresponds to the saline concentration of seawater). The value so calculated is further increased of 30% in order to avoid c_{Lout} being too high. In all scenarios, in order to avoid high values of c_{Lout} and of v_{Lin}/v_{Hin}, spacers with different thickness were considered for the two channels, i.e. 500 μm for the diluted compartments and 300 μm for the concentrated one. The scenarios may appear quite similar each other but the changing in the residence time induces a consistent variation in costs and energy consumption of the system for the dilution purpose. As it concerns the economic sensitivity analysis, the costs range assumed as input are reported in Tab. 4.

Tab. 4 Minimum, standard and maximum values of the main items considered for economic analysis.

	Min	Standard	Max
Water cost C_{water} [€ · m_w^{-3}]	0	0.1	0.3
Electricity cost $C_{electricity}$ [€ · kWh^{-1}]	0.12	0.12	0.22
Cost membrane C_m [€ · m_{IEMs}^{-2}]	4	10	15
Electrodes $C_{electrode}$ [€ · $m_{electrode}^{-2}$]	250	500	1000
Casing C_{casing} [€ · m_{IEMs}^{-2}]	2	2	5
Spacers C_{spacer} [€ · m_{IEMs}^{-2}]	2	5	10
Membrane life t_m [year]	7	4	2
Labour cost C_{labour} [% of equipment cost]	0.1	0.2	0.3
Other costs C_{other} [% of FCI]	2	4	6
Discount rate r [%]	0	3	6

Fig. 7 shows the behaviour of the system in scenario 1 considering a stack length of 0.5 m. Starting from the OCV conditions, with a voltage value of about 70 V and zero current, the external load is decreased up to reach the short circuit condition with an i_{SC}= 35 A·m^{-2} (see Fig. 7). While a small PW dilution is observed in OCV condition, given by the osmotic and diffusive flux, the maximum PW dilution in RED is obtained in short circuit condition with an outlet concentration of PW of about

55 g·L^{-1} (see Fig. 7c). In order to reach lower concentration values, the system can be operated in ARED conditions by applying an external electric field. In this case, an electric current of about 160 A·m^{-2} is required for obtaining the dilution target with an outlet PW concentration of 20 g·L^{-1} (Fig. 7c) by consuming a specific net energy (including the pumping energy) of about 8 kWh·m$^{-3}_{PW}$ (Fig. 7b). Moreover, a very low PW dilution is observed at the maximum power condition with a specific power produced of about 0.14 kWh·m$^{-3}_{PW}$.

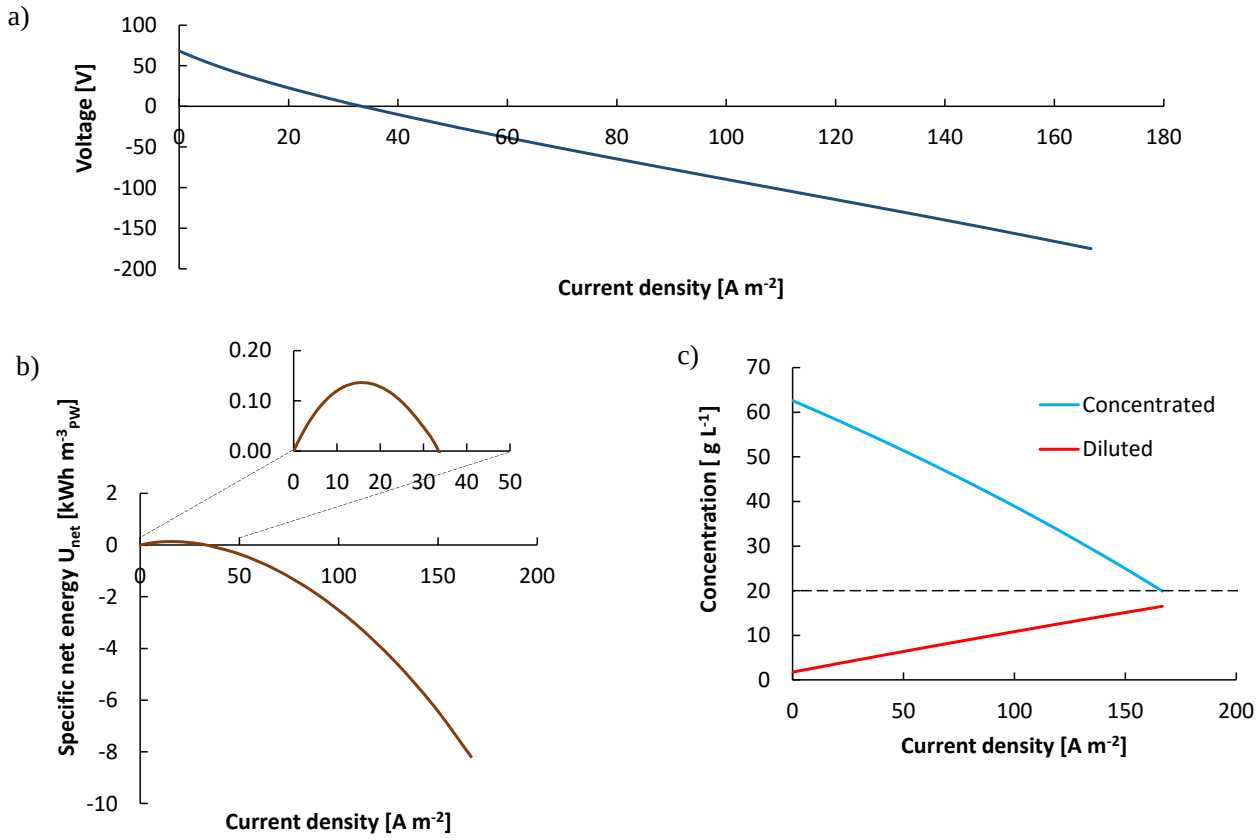

Fig. 7 Trends of voltage (a), outlet concentration of the two streams (b) and specific net energy (c) vs current density. Scenario 1 - L = 0.5 m.

In Fig. 8 it is shown the behaviour of the specific energy generated/consumed by the RED unit as a function of the PW outlet concentration (c_{Hout}) for six different stack lengths (in the range 0.5 – 4.0 m) for all the studied scenarios: scenario 1 (Fig. 8-a), scenario 2 (Fig. 8-b), scenario 3 (Fig. 8-c) and scenario 4 (Fig. 8-d).

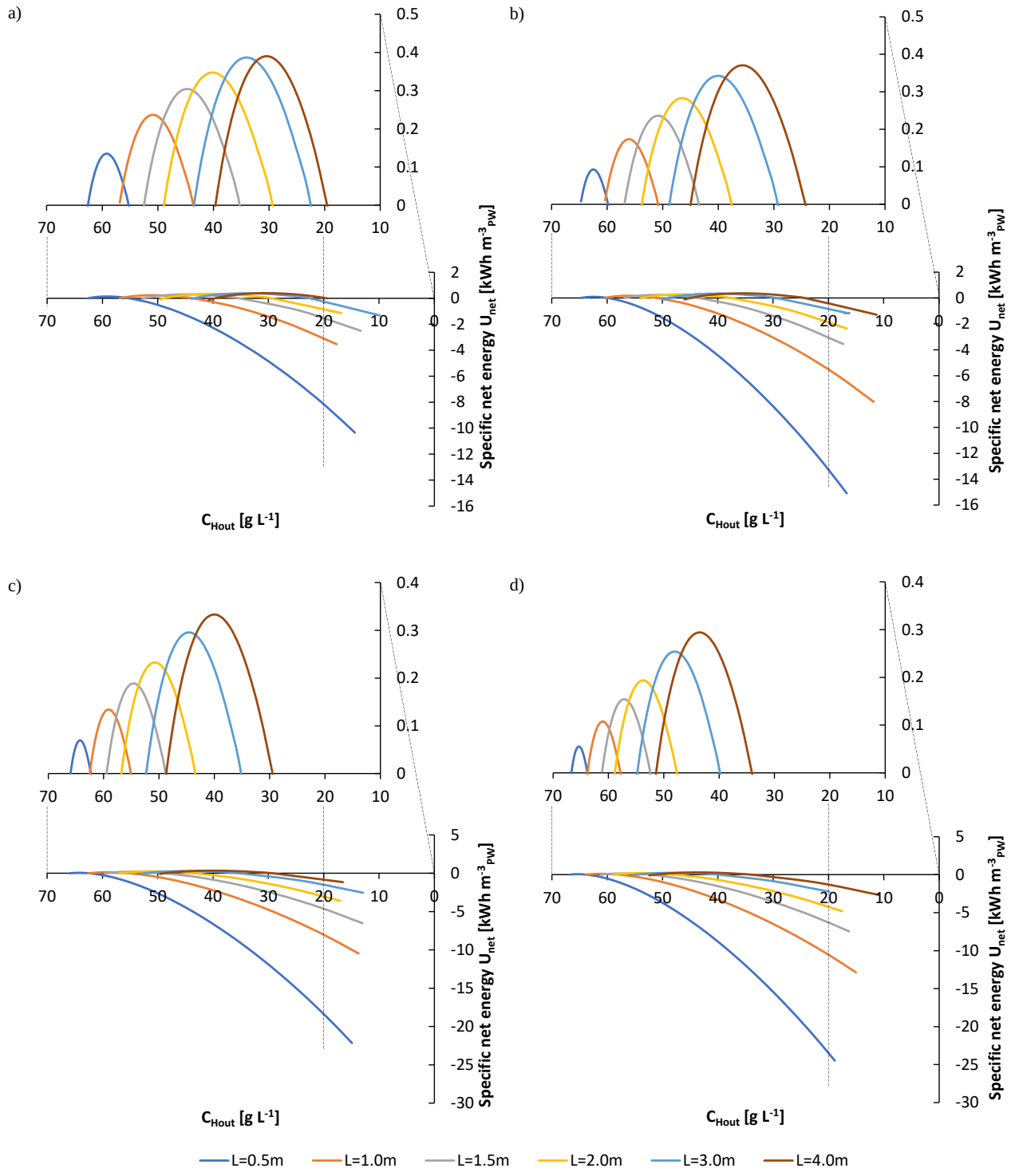

Fig. 8 Outlet concentration of H (i.e. the PWs) against the specific net energy U_{net} generated (RED mode) or required (ARED mode) at different stack lengths for scenario 1 (a), scenario 2 (b), scenario 3 (c) and scenario 4 (d). The vertical dashed line at 20 g L^{-1} indicates the dilution concentration target.

In all the investigated cases, the smaller the length of the stack, the greater the power required to dilute the PWs. A longer stack implies a higher residence time τ, shifting from a τ =125 s up to τ =1000 s when L is increased from 0.5 m up to 4 m in the scenario 1 and from τ =50 s to τ =400 s in

the scenario 4. As an example, when L =1 m the power required to reach the dilution target is equal to 3.1 kWh·m$^{-3}_{PW}$ in scenario 1 and 10.5 kWh·m$^{-3}_{PW}$ in scenario 4. Only in scenario 1 and for L = 4 m it is possible to achieve the dilution target by exploiting the natural salinity gradient between the two solutions, without supplying any external power. In all the other investigated cases, the target is obtained in ARED mode with the consumption of electric power.

The overall cost of the proposed treatment is the sum of (i) the annualized capital costs, which are strongly affected by the RED size and membrane cost, and (ii) the operative costs, which are largely affected by the operating conditions, and in particular, by the power required by the system when it is operated in ARED mode. In order to evaluate the most convenient plant configuration, a specific economic analysis was performed.

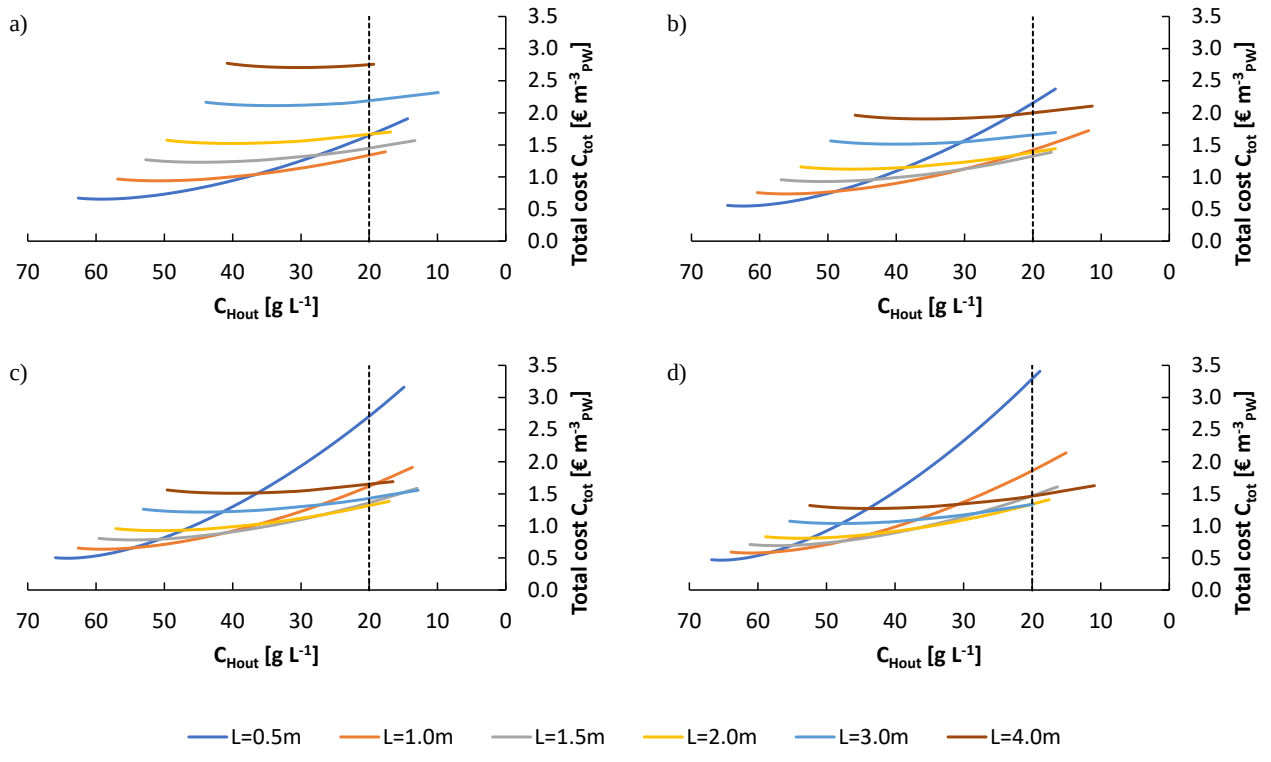

Fig. 9 Outlet concentration of PW (c_{Hout}) as a function of the dilution total specific cost at different stack lengths for scenario 1 (a), scenario 2 (b), scenario 3 (c) and scenario 4 (d). The vertical dashed line represents the dilution target of 20 g·L^{-1}. Standard economic inputs used are reported in Tab. 4.

Total specific cost (C_{tot}) required to dilute the PW down to its outlet concentration (c_{Hout}) for the scenarios described in Tab. 3 is reported in Fig. 9. Clearly, the higher the current density, the lower the membrane area required while the larger the energy supply needed (the latter for $i > i_{SC}$). These two competitive effects result into the non-monotonic behaviour of the curves (with a minimum cost) reported in Fig. 9. As already observed in Fig. 8, in all the investigated cases with the exception of scenario 1 - L= 4 m, which allows the achievement of the target in RED mode, the ARED operation mode is essential to economically reach the target. Indeed, a very expensive cost, (C_{tot} = 2.75 €·m^{-3}$_{PW}$ is required in RED mode).

Fig. 10 shows the Acapex and the Opex as a function of the stack length (current density and gross power) for the case of the scenario 1 configurations able to achieve the target. The Acapex increases linearly with *L* simply because the membrane area (the main Capex cost item) increases linearly with *L*. Conversely, the Opex trend is not linear: larger Opex can be found at low and high current density. At high current densities (i.e. target achievable with short stacks), Opex are dominated by the power to be spent in ARED conditions. At low current densities (i.e. target achievable with long stacks) Opex are high even in RED mode although no energy supply is needed. The latter is not surprising because Opex include other operating costs (i.e. C_{other}) which are calculated as 4% of FCI: thus, the larger the membrane/spacer area, the larger the FCI and the larger the Opex. Comparing Acapex and Opex, as expected, when the stack is operated in RED mode, the Acapex are consistent (about 55% of C_{tot}), especially for the high membrane cost (counting for the 34.3% of C_{tot}), making this operation mode prohibitive for the purpose of PW dilution. Conversely, for the ARED mode, the membrane cost, for the stack lengths considered, ranges from 7.2 to 24% of C_{tot}. Very interestingly, C_{tot} (i.e. the sum of Acapex and Opex) exhibits a minimum value for a stack length of 1 m which is the typical value of large scale RED stacks nowadays.

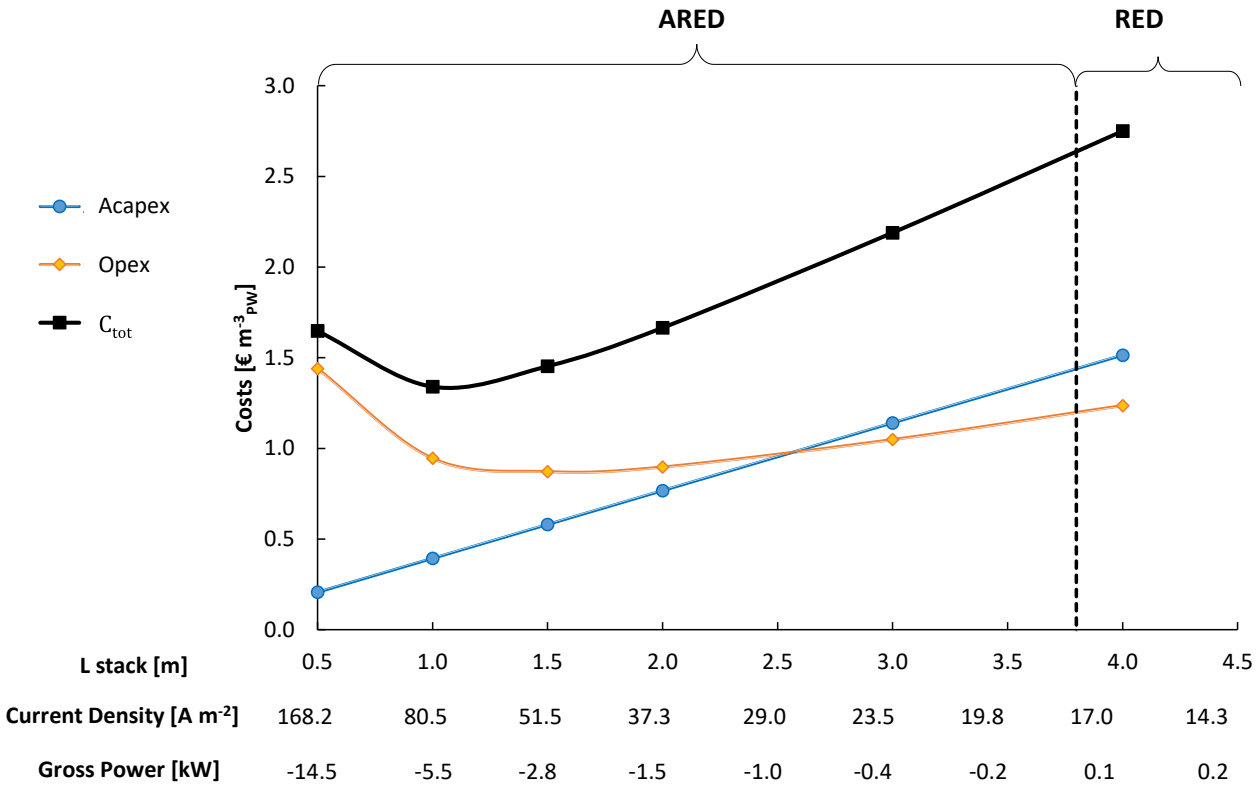

Fig. 10 Trend of the total specific cost C_{tot}, Acapex and Opex versus the stack length L, the current density and the gross power. The vertical dashed line represents short circuit current (I_{SC}) threshold value dividing the ARED and the RED operation mode zones. The graph is referred to scenario 1 and to the standard economic inputs of Tab. 4 by fixing c_{Hout}= 20 g·L^{-1}.

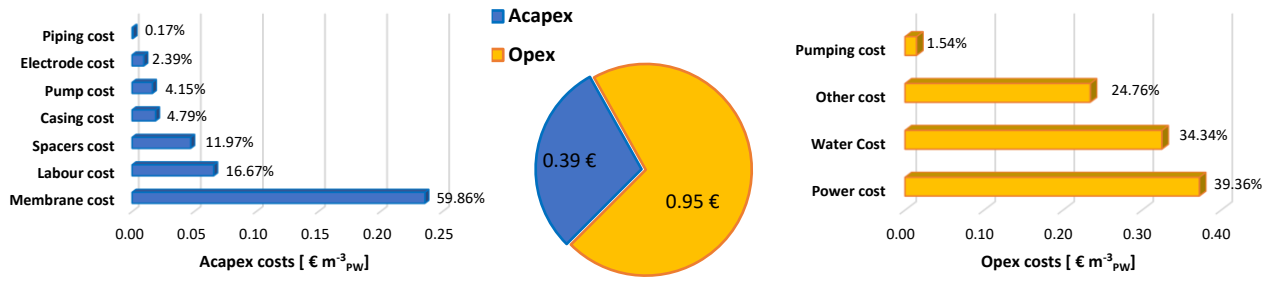

Fig. 11 Share of each cost item on the total specific cost C_{tot} specifically for Acapex and Opex for the minimum cost case (scenario 1 – L=1 m).

The impact of each cost item (on the economic minimum found in Fig. 10, scenario 1 – L=1 m) is shown in Fig. 11, where the target is achieved in ARED mode. As it can be observed, Opex counts

more than Acapex. Among Acapex, the membranes are the main cost (59.9%). Conversely, the power consumption is prominent among Opex (39.4%) and, alone, corresponds to 27.8% of C_{tot}.

In order to facilitate the comparison of the different scenarios, Fig. 12 shows the total specific cost C_{tot} required to obtain a concentration of PW equal to 20 g·L^{-1} as a function of the stack length and of the velocity. The ratio of the two parameters gives the residence time of the solution within the channels. When very small residence times are considered (i.e. for small stack and high v_{Hin}, i.e. $\tau <$ 100 s), the C_{tot} dramatically increases due to the significant amount of energy required by the system. Moreover, very high C_{tot} are obtained for the case of very high residence times (i.e. for long stack and small v_{Hin}, i.e. $\tau >$ 500 s) due to the significant impact of the cost related to the membrane surface. Interestingly, the lowest C_{tot} of about 1.32 €·m$^{-3}_{PW}$ is always observed at a residence time around 250 s.

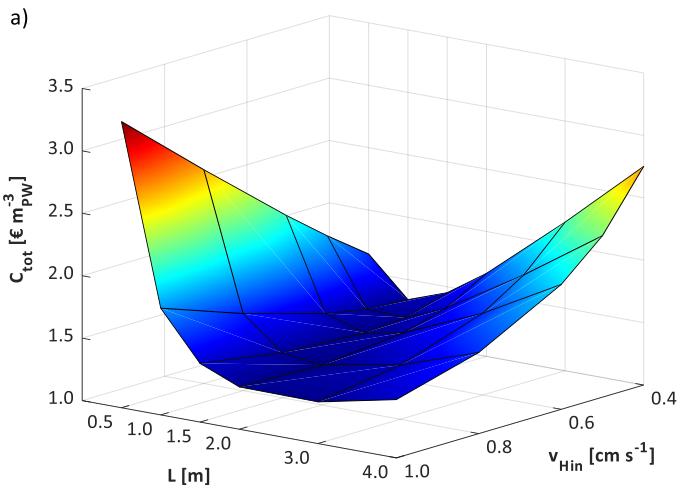

Stack Length L [m]	Concentrated velocity v_{Hin} [cm s^{-1}]			
	0.4	0.6	0.8	1.0
0.5	1.65	2.15	2.71	3.29
1.0	1.34	1.42	1.62	1.86
1.5	1.45	1.33	1.36	1.47
2.0	1.67	1.38	1.32	1.34
3.0	2.19	1.65	1.43	1.33
4.0	2.75	2.00	1.65	1.47

Fig. 12 Surface plot (a) and table of total costs (b) for all the scenarios considered varying the length of the stack, the costs are determined by fixing c_{Hout} = 20 g·L^{-1}.

With reference to the minimum cost configuration scenario 3 – L= 2 m , a sensitivity economic analysis was performed by adopting the different economic inputs described in Tab. 4. Fig. 13 shows this analysis in the form of a tornado diagram: economic parameters were changed singularly one after the other by keeping constant all the others in order to show how much the variation of each economic parameter may affect C_{tot}. Among the parameters under investigation, the main variation

is related to the cost of water C_{water}. There are a several industrial applications where water is abundantly available with practically no cost for using it. It is also very common for industries to have an own system to produce process water, which is rarely bought by an external provider. In our case, the water needed could derive from a mild treatment of a waste dilution stream available in the plant situ or even could be generated by a RO unit placed downstream the dilution and bioremediation units. In this regard, a maximum production cost of 0.3 €·m^{-3} of water is considered, thus leading the cost for treating a cubic meter of PWs to increase from about 1.32 €·m$^{-3}_{PW}$ up to 1.97 €·m$^{-3}_{PW}$ (i.e. + 49%).

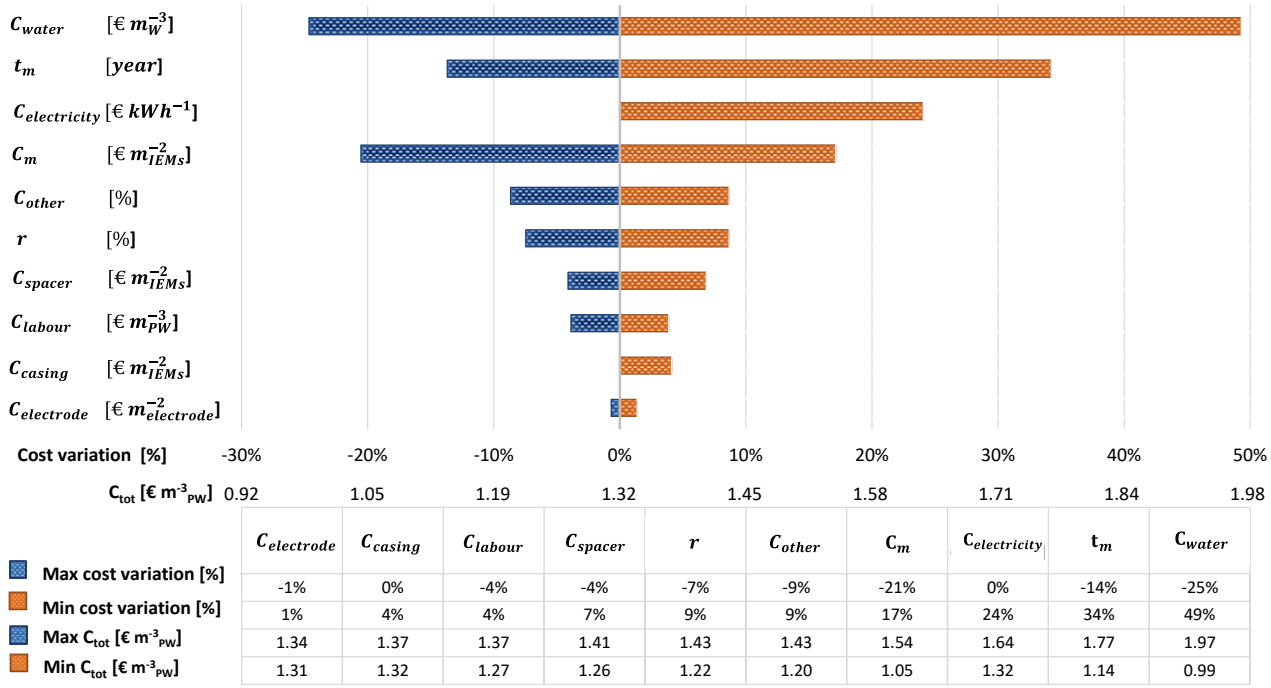

	$C_{electrode}$	C_{casing}	C_{labour}	C_{spacer}	r	C_{other}	C_m	$C_{electricity}$	t_m	C_{water}
Max cost variation [%]	-1%	0%	-4%	-4%	-7%	-9%	-21%	0%	-14%	-25%
Min cost variation [%]	1%	4%	4%	7%	9%	9%	17%	24%	34%	49%
Max C_{tot} [€ m$^{-3}_{PW}$]	1.34	1.37	1.37	1.41	1.43	1.43	1.54	1.64	1.77	1.97
Min C_{tot} [€ m$^{-3}_{PW}$]	1.31	1.32	1.27	1.26	1.22	1.20	1.05	1.32	1.14	0.99

Fig. 13 Tornado diagram and the relevant table representing the C_{tot} variation as a result of the cost ranges described in Tab. 4. The diagram refers to scenario 3 case exhibiting the lowest C_{tot} (scenario 3 – L= 2 m) in Fig. 12.

Also membrane cost and durability have a significant impact on the treatment process. In the standard case the cost was assumed equal to 10 €·m$^{-2}_{IEM}$, while according to [50], [51] a variation cost range of 4 and 15 €·m$^{-2}_{IEM}$ is assumed. The minimum membrane cost leads to a C_{tot} of 1.05 €·m$^{-3}_{PW}$ corresponding to a reduction of about 20%. Furthermore, an increase in membrane lifetime t_m from 4 to 7 years reduces C_{tot} to 1.14 €·m$^{-3}_{PW}$ (-14%). Conversely, reducing it to 2 years yields a cost variation of + 34%.

Electricity cost is another important parameter. A rise in the electric cost from the standard value of 0.12 €·kWh^{-1} up to 0.22 €·kWh^{-1} (+83 %), results in an increment of 24% of the total cost, especially when the stack operates in ARED condition. Finally, the variation of all the other parameters with respect to the standard values provides a variation of C_{tot} in the range ±10%.

Conclusions

PWs are wastewaters of oilfield production and represent a dramatic issue for the environment due to the huge production volumes and to the hydrocarbons pollutants which inhibit a safe disposal. For these reasons different methods are proposed in literature for the removal of pollutants. Biological reactors are known to be a cheap and efficient way to reduce drastically the quantity of hydrocarbons. Unfortunately, it is also well known that the typical high salinity of PWs inhibits the use of any bioremediation techniques. The traditional methods of water desalination are efficient and well-studied, although they are energy demanding and expensive. In this work RED and ARED technologies are proposed as methods to desalinate PWs in order to make them compliant with a downstream biological treatment. An ad-hoc tecno-economical multi-scale model is presented to reliably predict the controlled dilution capabilities and cost of RED/ARED units fed by PWs. The model is calibrated and validated with laboratory-scale experimental data purposely collected with real PWs resulting into correlations for the membrane permselectivity and electrical resistance more reliable than other ones available in literature.

The collected results indicate that among Acapex (annualized capital expenditures), membrane purchase is the main cost item, thus, the longer the stack to dilute the PW salinity down to the desired target value, the larger the Acapex. Among Opex (operating expenditures), utility (water and electricity) costs are prominent for short stacks operated in ARED mode, while other manufacturing costs (e.g. labour, maintenance, etc.) are significant for larger stacks as these are calculated as a percentage of the Fixed Capital Investment. Although RED can produce energy instead of consuming

it (as it occurs for ARED) and is able to reach the desalination target only in some cases, unfortunately, its corresponding dilution cost is prohibitive due to the high membrane area required.

The residence time plays a crucial role in the RED/ARED cost. A minimum in the cost to dilute a concentrated solution from 70 $g \cdot L^{-1}$ down to 20 $g \cdot L^{-1}$ was identified and found equal to about 1.32 € $\cdot m^{-3}_{PW}$. It was obtained for residence times of about 250 s, as a good compromise between the impact of Opex and Acapex. For residence times lower than 100 s the cost is dominated by the cost of the energy required while for residence time higher than 500 s it is dominated by the membrane cost. Interestingly, when the PW velocity is around 0.5 cm/s, the minimum dilution cost was found for a stack length of 1 m which is the typical value of large scale RED stacks nowadays.

Letting the cost of the main items to vary within a reasonable range (tornado diagram analysis), the total dilution cost was confirmed sensitive to water, electricity and membrane cost.

Overall, the cost values found in all cases appear reasonable and fully compatible with treatment chain devoted to PW treatment and valorisation whose tecno-economic assessment will be matter of a future work.

Appendices

Appendix I: Model equations

Model equations which were not reported in the main text for the sake of brevity are included in the following table:

Tab. 5 Model equations

CFD correlations			
Sherwood correlation [39], [40]	$Sh_{sol}(k) = (-1.48x10^{-7}Re^5 + 3.74x10^{-5}Re^4 - 3.25x10^{-3}Re^3 + 0.112Re^2 + 0.135Re + 6.95)(Sc/568)$	-	(A.1)
Reynold correlation	$Re(k) = \frac{\rho_{sol}\, u_{sol}\, (2\delta_{sp,sol})}{\mu_{sol}}$	-	(A.2)

Void velocity	$u_{sol} = \frac{v_{sol}}{(1 - f_{sp})}$	m·s^{-1}	(A.3)
	where f_{sp} is the relative spacer volume assumed 0.18		
Schimdt correlation	$Sc(k) = \frac{\mu_{sol}}{\rho_{sol} D_{sol}}$	-	(A.4)
Polarization factor of concentrated sol.	$\theta_H(k) = \frac{c_H^{int}}{C_H^b} = 1 - \frac{J_{salt}\,(2\delta_{sp,sol})}{Sh_H D_H c_H^b}$	-	(A.5)
Polarization factor of diluted sol.	$\theta_L(k) = \frac{c_L^b}{c_L^{int}} = \left[1 + \frac{J_{salt}\,(2\delta_{sp,sol})}{Sh_L D_L c_L^b}\right]^{-1}$	-	(A.6)
Pressure Drop	$\Delta p_{sol}(k) = \frac{1}{2} f_{fr,\ sol} \frac{\rho_{sol} u_{sol}^2 \Delta x}{2\delta_{sp,sol}}$	Pa	(A.7)
Friction factor [39], [40]	$f_{fr,\ sol} = (5.71x10^{-5}\ Re^2 + 2.64x10^{-2}\ Re + 6.6)\ 96/Re$	-	(A.8)

Transport Phenomena

Total salt flux	$J_{salt}(k) = J_{mig}(k) + J_{dif}(k)$	$mol \cdot m^{-2} \cdot s^{-1}$	(A.9)
Migrative salt flux	$J_{mig}(k) = \frac{i(k)}{F}$	$mol \cdot m^{-2} \cdot s^{-1}$	(A.10)
Diffusive salt flux	$J_{dif}(k) = \frac{2\ D_{NaCl}}{\delta_m}\left[c_H^{int}(k) - c_L^{int}(k)\right]$	$mol \cdot m^{-2} \cdot s^{-1}$	(A.11)
Interface concentration	$c_{sol}^{int}(k) = \theta_{sol}(k)\ c_{sol}^b$	$mol \cdot m^{-3}$	(A.12)
Water total flux	$J'_w(k) = J_{osm}(k) - J_{e-osm}(k)$	$m^3 \cdot m^{-2} \cdot s^{-1}$	(A.13)
Osmotic water flux	$J'_{osm}(k) = 2L_p(\Pi_H - \Pi_L)$ where the water permeability $L_p = 6.24$	$m^3 \cdot m^{-2} \cdot s^{-1}$ $mL\ (bar \cdot h \cdot m^2)^{-1}$	(A.14)
Electro-osmotic water flux	$J'_{e-osm}(k) = n_h\, J_{tot}(k) \frac{PM_w}{\rho_w}$ where the number of hydration of salt $n_h = 7$	$m^3 \cdot m^{-2} \cdot s^{-1}$	(A.15)
Osmotic pressure	$\Pi_{sol} = 2R_g T c_{sol}^{int} \varphi_{sol}$	Pa	(A.16)

Stack ohmic resistance

Cell resistance	$R_{cell}(k) = R_{AEM}(k) + R_H(k) + R_{CEM}(k) + R_L(k)$	$\Omega \cdot m^2$	(A.17)

Compartment resistance	$R_{sol}(k) = f_x \frac{\delta_{sp,sol}}{\sigma_{sol}}$ where f_x is the shadow factor along membrane equal to 1.56	$\Omega \cdot m^2$	(A.18)
Stack resistance	$R_{stack} = \frac{N_{cp}}{A_m}\left(\sum_{1}^{N_k} R_{cell}(k)\right) + \frac{R_{blank}}{A_m}$	Ω	(A.19)

Power and Energy

Gross power density	$P_{d,gross} = \frac{P_{gross}}{N_{cp} A_m}$	$W \cdot m^{-2}$	(A.20)
Pump power	$P_{pump} = \frac{1}{\eta_p}\left(Q_H \sum_{k}^{N_k} \Delta p_H(k) + Q_L \sum_{k}^{N_k} \Delta p_L(k)\right)$	$W \cdot m^{-2}$	(A.21)
Net power	$P_{net} = P_{gross} - P_{pump}$	W	(A.22)
Specific net energy	$U_{net} = \frac{P_{net}}{Q_H\ [m^3 \cdot h^{-1}]}$	$kWh \cdot m^{-3}{}_{PW}$	(A.23)

Appendix II: Solution properties

Salt diffusivity D :

The diffusivity is based on Vitignano and Lyons equation [58]:

For $c < 0.4$ $\quad D = 1.47x10^{-9} + 1.3x10^{-10}\exp(-c/70)$ (A.24)

For $c > 0.4$ $\quad D = -2.87262x10^{-21}c^3 + 2.0321x10^{-17}c^2 - 8.44113x10^{-15} + 1.4705x10^{-9}$ (A.25)

where c is the concentration of the salt solution expressed in $mol \cdot m^{-3}$. Diffusivity has $m^2 \cdot s^{-1}$ dimension.

Conductivity σ:

The conductivity correlation used in the Islam modified equation [59]:

$$\sigma = \left[\Lambda_0 - \frac{B_1\sqrt{c\prime}}{1+Ba_0\sqrt{c\prime}}\right]\left[1 - \frac{B_2 F\sqrt{c\prime}}{1+Ba_0\sqrt{c\prime}}\right] \cdot c' \quad (A.26)$$

where for a single-charged ion (as NaCl) is: $B = 50.29x10^8/\varepsilon_0 T^{0.5}$, $B_1 = 92.5/\mu_0\sqrt{\varepsilon_0 T}$, $B_2 = 8.204x10^5/\sqrt[2]{(\varepsilon_0 T)^3}$, $F = (\exp(0.2929B\sqrt{a_0}) - 1)/0.2929Ba_0\sqrt{c}$. Λ_0 is the equivalent conductance of the

aqueous NaCl solution (equal to 115 S·cm² at 25°C), μ_0 and ε_0 are the viscosity and the dielectric constant of water, T is the temperature and c' is the molar concentration of salt in mol·dm^{-3}. The conductivity so calculated has dimension of mS·cm^{-1}. The equation is referred to a NaCl aqueous solution and the advantages of using this correlation is the predictive ability to describe a wide range of salt concentrations.

Activity γ and osmotic φ coefficients:

For a binary system of singly charged ions, according to the Pitzer virial equation [60] the osmotic coefficients became:

$$\varphi - 1 = -A_1 \frac{\sqrt{m}}{1+ b'\sqrt{m}} + m\, B^{\varphi} + m^2\, C^{\varphi} \quad \text{(A.27)}$$

$$B^{\varphi} = \beta^{(0)} + \beta^{(1)} e^{-\alpha\sqrt{m}} \quad \text{(A.28)}$$

where m is the molality, A_1 is the modified Debye-Huckel constant (equal to 0.3915 at 25°C), α and b' are fixed constant equal respectively to 2 and 1.2 (kg·mol^{-1})$^{0.5}$ meanwhile $\beta^{(0)}$, $\beta^{(1)}$ and C^{φ} are functions of the electrolyte and for a NaCl aqueous solution are equal to 0.06743 , 0.3301 and 0.00263 respectively.

The activity coefficient can be obtained as:

$$\ln \gamma_{\pm} = -A_1 |z_+ z_-| \left[\frac{\sqrt{m}}{1+ b'\sqrt{m}} + \frac{2}{b'} \ln\left(1 + b'\sqrt{m}\right) \right] + m\, B^{\gamma} + m^2\, C^{\gamma} \quad \text{(A.29)}$$

where $|z_+ z_-|$ is the product between the valence of cations and anions, respectively. It is equal to 1 for NaCl. Meanwhile B^{γ}, C^{γ} are adjustable parameters and can be calculated as follow:

$$B^{\gamma} = 2\beta^{(0)} + 2\beta^{(1)} \left[1 - \left(1 + \alpha\sqrt{m} - \frac{\alpha^2}{2} m\right) e^{-\alpha\sqrt{m}}\right] \frac{1}{\alpha^2 m} \quad \text{(A.30)}$$

$$C^{\gamma} = \frac{3}{2} C^{\varphi} \quad \text{(A.31)}$$

Nomenclature

Symbols					
Acapex	€·year^{-1}	Annualized capital cost	Q	m^3·s^{-1}	Volumetric flow rate
			r	-	Discount rate

b	m	Width of stack	R	$\Omega \cdot m^2$	Generical resistance
c	$mol \cdot m^{-3}$	Molar concentration	R_g	$J \cdot mol^{-1} \cdot K^{-1}$	Universal gas constant
C	$€ \cdot unit^{-1}$	Cost	Re	-	Reynolds
D	$m^2 \cdot s^{-1}$	Diffusivity coefficient	Sc	-	Schimdt
E	V	Generical voltage	Sh	-	Sherwood
f_{fr}	-	Friction factor	t	year	Plant lifetime
f_{sp}	-	Relative spacer volume	T	K	Temperature
f_x	-	Shadow factor	u	$m \cdot s^{-1}$	Void velocity
F	$C \cdot mol^{-1}$	Faraday constant	v	$m \cdot s^{-1}$	Velocity
FCI	€	Fixed capital investment	z	-	Ion charge
i	$A \cdot m^{-2}$	Current density			
I	A	Current	**Greek letters**		
J	$mol \cdot m^{-2} \cdot s^{-1}$	Molar flux	γ	-	Activity coefficient
J’	$m^3 \cdot m^{-2} \cdot s^{-1}$	Volumetric flux	δ	m	Width
k	-	Iteration index	Δp	Pa	Pressure drop
L	m	Length of stack	Δx	m	Length step of discretization
L_p	$mL \cdot bar^{-1} \cdot h^{-1} \cdot m^{-2}$	Water permeability	θ	-	Polarization coefficient
n_h	-	Number of hydration of salt	Π	Pa	Osmotic pressure
N_{cp}	-	Number of cell pairs	μ	Pa s	Viscosity
N_k	-	Number of segments in discretization	ρ	$kg\ m^{-3}$	Density
Opex	$€ \cdot year^{-1}$	Operating expenditures	σ	$S\ m^{-1}$	Conductivity
P	W	Power	τ	s^{-1}	Residence time
PM	$g \cdot mol^{-1}$	Molecular weight	φ	-	Osmotic coefficient
PS	-	Permselectivity			

Subscripts/superscripts		**Acronyms/abbreviations**	
av	Average	ACC	Annual capital charge
b	Bulk	AEM	Anionic exchange membrane
d	Surface density	ARED	Assisted reverse electrodialysis
dif	Diffusive	Capex	Capital expenditures
e-osm	Electro-osmotic	CEM	Cationic exchange membrane
H	High concentration solution	ED	Electrodialysis
int	Interface membrane-solution	ERS	Electrodic rinse solution
L	Low concentration solution	HC	High solution compartment
m	Membrane	IEM	Ionic exchange membrane
mig	Migrative	LC	Low solution compartment
osm	Osmotic	MF	Microfiltration
sol	Solution (L or H)	MD	Membrane distillation
sp	Spacers	MSF	Multistage flash
tot	Total	OCV	Open circuit voltage

w	Water	PW	Produced water
out	Outlet	RED	Reverse electrodialysis
PW	Produced water	RO	Reverse osmosis
		SC	Short circuit
		UF	Ultrafiltration
		VCD	Vapor compression distillation

Acknowledgements

Mr Gianluca Ilardo is greatly acknowledged for his support during the experimental campaign.

References

[1] F.-R. Ahmadun, A. Pendashteh, L. C. Abdullah, D. R. A. Biak, S. S. Madaeni, and Z. Z. Abidin, "Review of technologies for oil and gas produced water treatment," Journal of Hazardous Materials, vol. 170, no. 2–3. pp. 530–551, Oct. 30, 2009. doi: 10.1016/j.jhazmat.2009.05.044.

[2] E. T. Igunnu and G. Z. Chen, "Produced water treatment technologies," International Journal of Low-Carbon Technologies, vol. 9, no. 3, pp. 157–177, 2014, doi: 10.1093/ijlct/cts049.

[3] S. Jiménez, M. M. Micó, M. Arnaldos, F. Medina, and S. Contreras, "State of the art of produced water treatment," Chemosphere, vol. 192. Elsevier Ltd, pp. 186–208, Feb. 01, 2018. doi: 10.1016/j.chemosphere.2017.10.139.

[4] M. A. Al-Ghouti, M. A. Al-Kaabi, M. Y. Ashfaq, and D. A. Da'na, "Produced water characteristics, treatment and reuse: A review," Journal of Water Process Engineering, vol. 28. Elsevier Ltd, pp. 222–239, Apr. 01, 2019. doi: 10.1016/j.jwpe.2019.02.001.

[5] I. Prihatiningtyas, A. H. A. H. Al-Kebsi, Y. Hartanto, T. M. Zewdie, and B. van der Bruggen, "Techno-economic assessment of pervaporation desalination of hypersaline water," Desalination, vol. 527, Apr. 2022, doi: 10.1016/j.desal.2021.115538.

[6] M. Wenzlick and N. Siefert, "Techno-economic analysis of converting oil & gas produced water into valuable resources," Desalination, vol. 481, May 2020, doi: 10.1016/j.desal.2020.114381.

[7] F. T. Tao et al., "Conversion of Oilfield Produced Water Into an Irrigation/Drinking Quality Water," 1993.

[8] M. M. M. Ali, H. Zhao, Z. Li, and N. N. M. Maglas, "Concentrations of TENORMs in the petroleum industry and their environmental and health effects," RSC Advances, vol. 9, no. 67. Royal Society of Chemistry, pp. 39201–39229, 2019. doi: 10.1039/c9ra06086c.

[9] D. J. Arthur, B. G. Langhus, and C. Patel, "TECHNICAL SUMMARY OF OIL & GAS PRODUCED WATER TREATMENT TECHNOLOGIES," 2005.

[10] K. S. Ashaghi, M. Ebrahimi, and P. Czermak, "Ceramic Ultra- and Nanofiltration Membranes for Oilfield Produced Water Treatment: A Mini Review," Open Environmental Sciences, vol. 1, pp. 1–8, 2007.

[11] M. Ebrahimi et al., "Innovative ceramic hollow fiber membranes for recycling/reuse of oilfield produced water," Desalination Water Treat, vol. 55, no. 13, pp. 3554–3567, Sep. 2015, doi: 10.1080/19443994.2014.947780.

[12] J. Mueller, Y. Cen, and R. H. Davis, "Crossflow microfiltration of oily water," J Memb Sci, vol. 129, pp. 221–235, 1997.

[13] E. Salehi, S. S. Madaeni, A. A. Shamsabadi, and S. Laki, "Applicability of ceramic membrane filters in pretreatment of coke-contaminated petrochemical wastewater: Economic feasibility study," Ceram Int, vol. 40, no. 3, pp. 4805–4810, Apr. 2014, doi: 10.1016/j.ceramint.2013.09.029.

[14] A. R. Pendashteh, L. C. Abdullah, A. Fakhru'L-Razi, S. S. Madaeni, Z. Zainal Abidin, and D. R. Awang Biak, "Evaluation of membrane bioreactor for hypersaline oily wastewater treatment," Process Safety and Environmental Protection, vol. 90, no. 1, pp. 45–55, Jan. 2012, doi: 10.1016/j.psep.2011.07.006.

[15] J. Drewes, T. Cath, J. Debroux, and J. Veil, "An Integrated Framework for Treatment and Management of Produced Water," 2009.

[16] O. A. Hamed, "EVOLUTIONARY DEVELOPMENTS OF THERMAL DESALINATION PLANTS IN THE ARAB GULF REGION 1," 2004.

[17] E. Jones, M. Qadir, M. T. H. van Vliet, V. Smakhtin, and S. mu Kang, "The state of desalination and brine production: A global outlook," Science of the Total Environment, vol. 657. Elsevier B.V., pp. 1343–1356, Mar. 20, 2019. doi: 10.1016/j.scitotenv.2018.12.076.

[18] S. Alzahrani, A. W. Mohammad, N. Hilal, P. Abdullah, and O. Jaafar, “Comparative study of NF and RO membranes in the treatment of produced water II: Toxicity removal efficiency,” Desalination, vol. 315, pp. 27–32, Apr. 2013, doi: 10.1016/j.desal.2012.12.014.

[19] S. Alzahrani, A. W. Mohammad, N. Hilal, P. Abdullah, and O. Jaafar, “Comparative study of NF and RO membranes in the treatment of produced water-Part I: Assessing water quality,” Desalination, vol. 315, pp. 18–26, Apr. 2013, doi: 10.1016/j.desal.2012.12.004.

[20] S. Mondal and S. R. Wickramasinghe, “Produced water treatment by nanofiltration and reverse osmosis membranes,” J Memb Sci, vol. 322, no. 1, pp. 162–170, Sep. 2008, doi: 10.1016/j.memsci.2008.05.039.

[21] A. Matin, T. Laoui, W. Falath, and M. Farooque, “Fouling control in reverse osmosis for water desalination & reuse: Current practices & emerging environment-friendly technologies,” Science of the Total Environment, vol. 765. Elsevier B.V., Apr. 15, 2021. doi: 10.1016/j.scitotenv.2020.142721.

[22] D. L. Shaffer, L. H. Arias Chavez, M. Ben-Sasson, S. Romero-Vargas Castrillón, N. Y. Yip, and M. Elimelech, “Desalination and reuse of high-salinity shale gas produced water: Drivers, technologies, and future directions,” Environmental Science and Technology, vol. 47, no. 17. pp. 9569–9583, Sep. 02, 2013. doi: 10.1021/es401966e.

[23] E. Curcio and E. Drioli, “Membrane distillation and related operations - A review,” Separation and Purification Reviews, vol. 34, no. 1. pp. 35–86, 2005. doi: 10.1081/SPM-200054951.

[24] A. Campione, L. Gurreri, M. Ciofalo, G. Micale, A. Tamburini, and A. Cipollina, “Electrodialysis for water desalination: A critical assessment of recent developments on process fundamentals, models and applications,” Desalination, vol. 434. Elsevier B.V., pp. 121–160, May 15, 2018. doi: 10.1016/j.desal.2017.12.044.

[25] M. Fidaleo and M. Moresi, “Electrodialysis Applications in The Food Industry,” Adv Food Nutr Res, vol. 51, pp. 265–360, 2006, doi: 10.1016/S1043-4526(06)51005-8.

[26] H. Strathmann, “Electrodialysis, a mature technology with a multitude of new applications,” Desalination, vol. 264, no. 3, pp. 268–288, Dec. 2010, doi: 10.1016/j.desal.2010.04.069.

[27] M. A. Acheampong, R. J. W. Meulepas, and P. N. L. Lens, “Removal of heavy metals and cyanide from gold mine wastewater,” Journal of Chemical Technology and Biotechnology, vol. 85, no. 5. pp. 590–613, May 2010. doi: 10.1002/jctb.2358.

[28] C. R. Gally et al., “Electrodialysis for the tertiary treatment of municipal wastewater: Efficiency of ion removal and ageing of ion exchange membranes,” J Environ Chem Eng, vol. 6, no. 5, pp. 5855–5869, Oct. 2018, doi: 10.1016/j.jece.2018.07.052.

[29] L. Gurreri, M. la Cerva, J. Moreno, B. Goossens, A. Trunz, and A. Tamburini, “Coupling of electromembrane processes with reverse osmosis for seawater desalination: Pilot plant demonstration and testing,” Desalination, vol. 526, Mar. 2022, doi: 10.1016/j.desal.2021.115541.

[30] A. Cosenza et al., “Power Production from Produced Waters via Reverse Electrodialysis: A Preliminary Assessment,” Energies (Basel), vol. 15, no. 11, p. 4177, Jun. 2022, doi: 10.3390/en15114177.

[31] P. Ma, X. Hao, F. Proietto, A. Galia, and O. Scialdone, “Assisted reverse electrodialysis for CO2 electrochemical conversion and treatment of wastewater: A new approach towards more eco-friendly processes using salinity gradients,” Electrochim Acta, vol. 354, Sep. 2020, doi: 10.1016/j.electacta.2020.136733.

[32] M. Vanoppen, E. Criel, G. Walpot, D. A. Vermaas, and A. Verliefde, “Assisted reverse electrodialysis—principles, mechanisms, and potential,” NPJ Clean Water, vol. 1, no. 1, Dec. 2018, doi: 10.1038/s41545-018-0010-1.

[33] M. la Cerva, L. Gurreri, A. Cipollina, A. Tamburini, M. Ciofalo, and G. Micale, “Modelling and cost analysis of hybrid systems for seawater desalination: Electromembrane pre-treatments for Reverse Osmosis,” Desalination, vol. 467, pp. 175–195, Oct. 2019, doi: 10.1016/j.desal.2019.06.010.

[34] W. Li, W. B. Krantz, E. R. Cornelissen, J. W. Post, A. R. D. Verliefde, and C. Y. Tang, “A novel hybrid process of reverse electrodialysis and reverse osmosis for low energy seawater desalination and brine management,” Appl Energy, vol. 104, pp. 592–602, 2013, doi: 10.1016/j.apenergy.2012.11.064.

[35] Q. Wang et al., “Hybrid RED/ED system: Simultaneous osmotic energy recovery and desalination of high-salinity wastewater,” Desalination, vol. 405, pp. 59–67, Mar. 2017, doi: 10.1016/j.desal.2016.12.005.

[36] R. E. Pattle, “Pattle - Production of electric power by mixing fresh and salt water in the hydro-electric pile,” Nature, vol. 174, 1954.

[37] J. Veerman, M. Saakes, S. J. Metz, and G. J. Harmsen, “Reverse electrodialysis: A validated process model for design and optimization,” Chemical Engineering Journal, vol. 166, no. 1, pp. 256–268, Jan. 2011, doi: 10.1016/j.cej.2010.10.071.

[38] M. Tedesco, A. Cipollina, A. Tamburini, I. D. L. Bogle, and G. Micale, “A simulation tool for analysis and design of reverse electrodialysis using concentrated brines,” Chemical Engineering Research and Design, vol. 93, pp. 441–456, Jan. 2015, doi: 10.1016/j.cherd.2014.05.009.

[39] L. Gurreri, A. Tamburini, A. Cipollina, G. Micale, and M. Ciofalo, “CFD prediction of concentration polarization phenomena in spacer-filled channels for reverse electrodialysis,” J Memb Sci, vol. 468, pp. 133–148, Oct. 2014, doi: 10.1016/j.memsci.2014.05.058.

[40] M. L. la Cerva et al., “Coupling CFD with a one-dimensional model to predict the performance of reverse electrodialysis stacks,” J Memb Sci, vol. 541, pp. 595–610, Jan. 2017, doi: 10.1016/j.memsci.2017.07.030.

[41] A. Culcasi et al., “Ionic shortcut currents via manifolds in reverse electrodialysis stacks,” Desalination, vol. 485, Jul. 2020, doi: 10.1016/j.desal.2020.114450.
[42] D. Pintossi, C. Simões, M. Saakes, Z. Borneman, and K. Nijmeijer, “Predicting reverse electrodialysis performance in the presence of divalent ions for renewable energy generation,” Energy Convers Manag, vol. 243, Sep. 2021, doi: 10.1016/j.enconman.2021.114369.
[43] A. Culcasi, L. Gurreri, G. Micale, and A. Tamburini, “Bipolar membrane reverse electrodialysis for the sustainable recovery of energy from pH gradients of industrial wastewater: Performance prediction by a validated process model,” J Environ Manage, vol. 287, Jun. 2021, doi: 10.1016/j.jenvman.2021.112319.
[44] C. Tristán, M. Fallanza, R. Ibáñez, and I. Ortiz, “Recovery of salinity gradient energy in desalination plants by reverse electrodialysis,” Desalination, vol. 496, Dec. 2020, doi: 10.1016/j.desal.2020.114699.
[45] V. M. Ortiz-Martínez et al., “A comprehensive study on the effects of operation variables on reverse electrodialysis performance,” Desalination, vol. 482, May 2020, doi: 10.1016/j.desal.2020.114389.
[46] R. Ortiz-Imedio, L. Gomez-Coma, M. Fallanza, A. Ortiz, R. Ibañez, and I. Ortiz, “Comparative performance of Salinity Gradient Power-Reverse Electrodialysis under different operating conditions,” Desalination, vol. 457, pp. 8–21, May 2019, doi: 10.1016/j.desal.2019.01.005.
[47] A. Cosenza, D. di Trapani, G. Mannina, S. Nicosia, M. Torregrossa, and G. Viviani, “Comparison between two MBR pilot plants treating synthetic shipboard slops: the effect of salinity increase on biological performance, biomass activity and fouling tendency,” Desalination Water Treat, vol. 61, pp. 240–249, Jan. 2017, doi: 10.5004/dwt.2017.11123.
[48] G. Mannina, M. Capodici, A. Cosenza, D. di Trapani, and G. Viviani, “Sequential batch membrane bio-reactor for wastewater treatment: The effect of increased salinity,” Bioresour Technol, vol. 209, pp. 205–212, Jun. 2016, doi: 10.1016/j.biortech.2016.02.122.
[49] D. A. Vermaas, E. Guler, M. Saakes, and K. Nijmeijer, “Theoretical power density from salinity gradients using reverse electrodialysis,” Energy Procedia, vol. 20, pp. 170–184, 2012, doi: 10.1016/j.egypro.2012.03.018.
[50] A. Daniilidis, R. Herber, and D. A. Vermaas, “Upscale potential and financial feasibility of a reverse electrodialysis power plant,” Appl Energy, vol. 119, pp. 257–265, Apr. 2014, doi: 10.1016/j.apenergy.2013.12.066.
[51] F. Giacalone, M. Papapetrou, G. Kosmadakis, A. Tamburini, G. Micale, and A. Cipollina, “Application of reverse electrodialysis to site-specific types of saline solutions: A techno-economic assessment,” Energy, vol. 181, pp. 532–547, Aug. 2019, doi: 10.1016/j.energy.2019.05.161.
[52] S. Quoilin, S. Declaye, B. F. Tchanche, and V. Lemort, “Thermo-economic optimization of waste heat recovery Organic Rankine Cycles,” Appl Therm Eng, vol. 31, no. 14–15, pp. 2885–2893, 2011, doi: 10.1016/j.applthermaleng.2011.05.014.
[53] Y. D. Raka, H. Karoliussen, K. M. Lien, and O. S. Burheim, “Opportunities and challenges for thermally driven hydrogen production using reverse electrodialysis system,” Int J Hydrogen Energy, vol. 45, no. 2, pp. 1212–1225, Jan. 2020, doi: 10.1016/j.ijhydene.2019.05.126.
[54] R. Sinnott and G. Towler, Chemical Engineering Design. Elsevier, 2019. doi: 10.1016/B978-0-08-102599-4.09980-X.
[55] E. Fontananova et al., “Effect of solution concentration and composition on the electrochemical properties of ion exchange membranes for energy conversion,” J Power Sources, vol. 340, pp. 282–293, Feb. 2017, doi: 10.1016/j.jpowsour.2016.11.075.
[56] J. Moreno, S. Grasman, R. van Engelen, and K. Nijmeijer, “Upscaling Reverse Electrodialysis,” Environ Sci Technol, vol. 52, no. 18, pp. 10856–10863, Sep. 2018, doi: 10.1021/acs.est.8b01886.
[57] D. Jin, R. Xi, S. Xu, P. Wang, and X. Wu, “Numerical simulation of salinity gradient power generation using reverse electrodialysis,” Desalination, vol. 512, Sep. 2021, doi: 10.1016/j.desal.2021.115132.
[58] V. Vitignano and P. A. Lyons, “Diffusion coefficients for aqueous solutions of sodium chloride and barium chloride,” 1955.
[59] S. S. Islam, R. L. Gupta, and K. Ismall’, “Extension of the Falkenhagen-Leist-Kelbg Equation to the Electrical Conductance of Concentrated Aqueous Electrolyte,” J. Chem. Eng. Data, vol. 36, pp. 102–104, 1991.
[60] J. I. Partanen, “Traceable mean activity coefficients and osmotic coefficients in aqueous calcium chloride solutions at 25 °c up to a molality of 3.0 mol·kg-1,” J Chem Eng Data, vol. 57, no. 11, pp. 3247–3257, Nov. 2012, doi: 10.1021/je300852v.